Florida International University
Technical Report

USING SMOOTHED SOUND SPEED TO REDUCE CHAOTICITY OF CHAOS IN OCEAN ACOUSTICS

PREPARED UNDER THE GRANT (N00014-97-1-0518) FROM THE OFFICE OF NAVAL RESEARCH

Kang K. Yen, Jianguo Yan

April 1998

REPORT DOCUMENTATION PAGE

Form Approved
OMB No. 0704-0188

1. AGENCY USE ONLY (Leave blank)	2. REPORT DATE	3. REPORT TYPE AND DATES COVERED
	July 31, 1998	

4. TITLE AND SUBTITLE

Overcoming Ray Chaos in Ocean Acoustics

5. FUNDING NUMBERS

N00014-97-10518

6. AUTHOR(S)

Kang, K. Yen, Jianguo Yan

7. PERFORMING ORGANIZATION NAME(S) AND ADDRESS(ES)

Florida International University
Department of Electrical and Computer Engineering
Miami, FL 33199

8. PERFORMING ORGANIZATION REPORT NUMBER

9. SPONSORING / MONITORING AGENCY NAME(S) AND ADDRESS(ES)

Office of Naval Research
800 North Quincy Street, Ballston Tower One
Arlington, VA 22217-5660

10. SPONSORING / MONITORING AGENCY REPORT NUMBER

11. SUPPLEMENTARY NOTES

12a. DISTRIBUTION / AVAILABILITY STATEMENT

Approved for public release; distribution unlimited.

12b. DISTRIBUTION CODE

13. ABSTRACT (Maximum 200 words)

Chaos has been shown in the previous project (N00014-95-10443) to exhibit in three- dimensional (3-D) ray tracing for long-range acoustic transmissions in the ocean. It imposes a limitation on our ability to make long-range predictions. We have previously found that the sound speed fluctuations in the upper ocean might be a reason for large chaoticity. Therefore, we inferred that a smoothed sound speed field could reduce chaoticity and thus improve predictability. This hypothesis is tested and confirmed in this project. We still study the Heard-to-Ascension sound propagation, which has shown large chaoticity and extremely limited predictability, in our previous work, when NODC measured sound speed data were used. In this work, the same NODC data were smoothed by using a sound speed model, so that the sound speed fluctuations in both longitude direction and depth direction are ignored. We use the smoothed sound speed to perform 3-D ray tracing. Numerical results show that chaoticity was significantly reduced and consequently predictability greatly improved. The ray paths show a pattern similar to those constructed using the original NODC data. The travel times, however, were less than the previous results by about 10 seconds, with a relative error of 0. 16%. This error was produced by the smoothed sound speed.

14. SUBJECT TERMS

Chaos Underwater Sound
Acoustics

15. NUMBER OF PAGES

76

16. PRICE CODE

17. SECURITY CLASSIFICATION OF REPORT	18. SECURITY CLASSIFICATION OF THIS PAGE	19. SECURITY CLASSIFICATION OF ABSTRACT	20. LIMITATION OF ABSTRACT
Unclassified	Unclassified	Unclassified	UL

Abstract

Chaos has been shown in the previous project (N00014-95-10443) to exhibit in three- dimensional (3-D) ray tracing for long-range acoustic transmissions in the ocean. It imposes a limitation on our ability to make long-range predictions. We have previously found that the sound speed fluctuations in the upper ocean might be a reason for large chaoticity. Therefore, we inferred that a smoothed sound speed field could reduce chaoticity and thus improve predictability. This hypothesis is tested and confirmed in this project. We still study the Heard-to-Ascension sound propagation, which has shown large chaoticity and extremely limited predictability, in our previous work, when NODC measured sound speed data were used. In this work, the same NODC data were smoothed by using a sound speed model, so that the sound speed fluctuations in both longitude direction and depth direction are ignored. We use the smoothed sound speed to perform 3-D ray tracing. Numerical results show that chaoticity was significantly reduced and consequently predictability greatly improved. The ray paths show a pattern similar to those constructed using the original NODC data. The travel times, however, were less than the previous results by about 10 seconds, with a relative error of 0. 16%. This error was produced by the smoothed sound speed.

Table of Contents

1. Introduction

Chaos is defined to be aperiodic bounded dynamics in a deterministic system with sensitive dependence on initial conditions.[1] In 1988, Palmer et al.[2] demonstrated that chaos appeared in two-dimensional (2-D) acoustic ray tracing in the ocean. It is then called "ray chaos" by the ocean acoustics community and further studies [3,4,5,6,7,8,9,10,11] have been performed following the Palmer et al.'s work.

These previous studies are important. However, they all deal with 2-D ray tracing. The 2-D equations are not valid for long-range transmissions, while ray chaos is a phenomenon in long-range sound propagation. In other words, the 2-D equations may lose validity before chaos is manifest. This can be seen from Smith et al.'s work.[8] In that work, a predictability horizon of 1000 to 2000 km has been estimated by using Lyapunov exponents, but the ray equations used in that work are only valid for about 100 km. This implies that the predictability was limited by the validity of the 2-D ray equations, rather than chaos.

For long-range transmissions, we currently have three sets of ray equations. They are horizontal ray equations,[12,13] Hamiltonian equations in HARPO,[14] and 3-D ray equations in ellipsoidal coordinates.[15] These equations are valid for very long ranges. Chaos may be a major factor that determines the predictability of these ray models. Therefore, we need to used these models to study chaos to understand our ability to make long-range predictions. We have recently studied chaos in horizontal ray tracing,[16]and

then in the previous project (ONR Grant N00014-95-10443), we have studied chaos in 3-D ray tracing.[17,18,19]

We have studied two 3-D cases in the previous work.[17,19] The first is the Heard-to-Ascension (H-A) sound propagation, and the second is the California-to-Hawaii (C-H) propagation. Chaos appeared in both cases. However, there was a significant difference between the two cases. In the H-A case, chaoticity was very strong, and predictability was extremely limited by chaos, In the C-H case, however, chaos was weak, and predictions were made with high precision. Comparison between the two cases suggests that there is an apparent difference in sound speed data, besides the difference in propagation range. The sound speed data used for the H-A sound propagation have large fluctuation in the upper ocean, as can be seen from Fig. 1. The sound speed fluctuation in the C-H case, however, is very small, as seen from Fig. 2. Therefore, the smoothness of the sound speed data in the C-H case might be a reason for the weak chaos. This leads to a hypothesis: a smoothed sound speed field can reduce chaoticity and thus enhance our ability to make long-range predictions.[17'19]

The objective of this project is to test this hypothesis. To study the feasibility of using smoothed sound speed data to reduce chaoticity, we tackle the H-A problem that had very large chaoticity in our previous work.[17,19] We use the same sound speed data as those used in our previous work, but before ray-tracing we fit the data to a mathematical model and use the model to provide a smoothed sound speed field. This is described in section two. In section three, we use the smoothed sound speed data to perform ray

tracing, and use Lyapunov exponent to quantify chaoticity. The numerical results will be compared with those of our previous work to test the feasibility of the proposed method. In section four, presented are summary and discussions. We focus on the correctness of the ray tracing, considering that the smoothed sound speed field might lose reality, which could in turn affect the correctness of ray tracing. We wonder if there is a compromise between an improved predictability and the correctness of ray-tracing results.

2. Smoothing Sound Speed Data with Munk's Model

2.1 Characteristics of Sound Speed Profiles

From the sound speed data provided by the National Oceanic Data Center (NODC), we can see that

- the sound speed fluctuates at the upper ocean, and
- for a given latitude, the sound speed profiles (SSP) at different longitude are similar in shape.

These characteristics can be seen, for example, from Fig. 1. We have studied all the NODC data for the Southern Atlantic Ocean, and this is true for all the data files we have received from NODC, as depicted in the Appendix.

The first characteristic might be a major factor that causes chaos in ray tracing. The second characteristic, however, may lead to a method to reduce chaoticity. It allows us to use a model to approximate all the SSP for a given latitude. In this way, we can

smooth the NODC sound speed data to reduce chaoticity. Such a model is implemented as follows.

2.2 Fitting Data to Munk's Canonical Model

In ocean acoustics, Munk[20] has presented a sound speed model expressed as

$$c(r) = c_a\left[1 + \varepsilon\left(\eta + e^{-\eta} - 1\right)\right], \tag{1}$$

where

$$\eta = 2\left(r - r_a\right) / B. \tag{2}$$

Here c is the sound speed; r is the depth; c_a and r_a are the sound speed and the depth at channel axis, respectively; B is the scale depth; ε is the perturbation coefficient; and η is a dimensionless distance. This model is commonly considered as a model for deep ocean. By plotting the NODC data, however, we note that for a given latitude, all the sound speed profiles including shallow water SSP are similar in shape, except that they terminate at different depths. This suggests that we can use Munk's model to approximate all the SSP for a given latitude. This can be done by fitting the NODC measured sound speed data to Munk's model, described as follows.

Let c be the sound speed computed using Munk's model, and C be the NODC measured data. Then, the difference between the model output and the measured data can be quantified using

$$M(\mathbf{x}) = \sum_{i=1}^{N}\sum_{j=1}^{n}\left[c(\mathbf{x})_j - C_j\right]_i^2, \tag{3}$$

Equation (3) means that we have N SSP for a given latitude, and each SSP is sampled at n depth points. Here, the depth is not equally discretized. The NODC data have the standard depths listed in Table 1. In Eq. (3), **x** represents the model parameters in Eq. (1) and (2), i.e., $c_a, \varepsilon, \eta, r_a$, and B.

Now we can fit the NODC measured data to Munk's model by solving the following problem:

$$\text{Minimize } \{M(x)\}, \tag{4}$$

subject to the constraints

$$\begin{aligned} c_a^l < c_a < c_a^u, \\ \varepsilon^l < \varepsilon < \varepsilon^u, \\ \eta^l < \eta < \eta^u, \\ r_a^l < r_a < r_a^u, \\ B^l < B < B^u, \end{aligned} \tag{5}$$

where superscript l represents the lower bound of the parameter, and u the upper bound. In the following calculations, we use $0 < \varepsilon < 0.01$, and $0.4 < B < 1.7$. The ranges of c_a and r_a vary substantially with latitudes, and thus are determined directly from the plots of the measured NODC data in the Appendix.

Problem (4) is a constrained optimization problem, and can be solved using the Complex method.[21,22] Using this method, we can estimate the model parameters in Eqs.(1) and (2). We have NODC measured sound speed data of the Southern Atlantic Ocean. The latitude of the data ranges from 8°S to 52°S with 1° increment. We first sort the NODC data into numerical orders of latitudes, and get 45 data sets corresponding to

45 latitudes. Then we fit each data set in Munk's model (1) using the Complex method of optimization. The model parameters estimated are listed in Table 2.

Figure 3 shows typical results of fitting the NODC data to Munk's model. We can see that the model predictions are in good agreement with the NODC measured data, not only at low latitude (Fig. 3-1), but also at high latitude (Fig. 3-2). For mid-latitudes, however, the discrepancy between the NODC data and the model predictions is larger (Fig. 3-3). This is because that the measured data fluctuated substantially at these latitudes. The output of Munk's model is still a good approximation as an averaged SSP.

2.3 A Sound Speed Model of Southern Atlantic Ocean

By fitting the NODC measured sound speed data to Munk's model, we can now use Eq. (1) to approximate all the SSP for a given latitude. In this way, we can smooth the sound speed in both the longitude direction and the depth direction. Suppose that the sound speed data are sampled at N different latitudes, expressed as $\phi_1, \phi_2, \ldots, \phi_N$. Then we have N sound speed profiles, $c(r)_1, c(r)_2, \ldots, c(r)_N$, which can be approximated using Eq. (1). For a latitude located between ϕ_i and ϕ_{i+1}, the sound speed can be calculated using the linear interpolation between $c(r)_i$ and $c(r)_{i+1}$, i.e.,

$$c(\phi, r) = c(r)_i + \frac{c(r)_{i+1} - c(r)_i}{\phi_{i+1} - \phi_i}(\phi - \phi_i) \qquad (6)$$

Equation (6) is a sound speed model we shall use to perform ray tracing for Heard-to-Ascension sound propagation. This model ignores the sound speed fluctuations in both the longitude and the depth direction. It might be a good approximation considering that

these fluctuations are relatively small compared with that in the latitude direction. We shall investigate the feasibility of using this model to improve the predictability of ray tracing, and discuss the correctness of this model in section four.

3. Numerical Ray Tracing

We have just formulated a sound speed model for the Southern Atlantic Ocean. The model smoothes the NODC measured sound speed data in both the longitude direction and the depth direction. Now we use this model for ray tracing. We have two objectives. First, we test the hypothesis: a smoothed sound speed field can reduce chaoticity, and improve predictability. Second, we examine the correctness of the ray tracing—we wonder if the smoothed sound speed field is a good approximation to reality.

3.1 Methods

For comparison, we still use the 3-D ray equations that we used in our previous work (17,19). They are

$$\frac{d\phi}{ds} = \frac{\cos\theta\cos\alpha}{\mu - r}, \tag{7}$$

$$\frac{d\lambda}{ds} = \frac{\cos\theta\sin\alpha}{(\nu - r)\cos\phi}, \tag{8}$$

$$\frac{dr}{ds} = \sin\theta, \tag{9}$$

$$\frac{d\alpha}{ds} = \frac{\cos\theta\tan\phi\sin\alpha}{\nu - r} + \sin\theta\sin\alpha\cos\alpha\left(\frac{1}{\nu - r} - \frac{1}{\mu - r}\right) + \left(-\frac{\sin\alpha}{\mu - r}\frac{\partial}{\partial\phi} + \frac{\cos\alpha}{(\nu - r)\cos\phi}\frac{\partial}{\partial\lambda}\right)\frac{\ln N}{\cos\theta}, \tag{10}$$

and

$$\frac{d\theta}{ds} = -\cos\theta\left(\frac{\sin^2\alpha}{\nu - r} + \frac{\cos^2\alpha}{\mu - r}\right) + \left(-\frac{\sin\theta\cos\alpha}{\mu - r}\frac{\partial}{\partial\phi} - \frac{\sin\theta\sin\alpha}{(\nu - r)\cos\phi}\frac{\partial}{\partial\lambda} + \cos\theta\frac{\partial}{\partial r}\right)\ln N, \tag{11}$$

where

$$\mu = \frac{a(1 - e^2)}{(1 - e^2\sin^2\phi)^{3/2}}, \tag{12}$$

and

$$\nu = \frac{a}{(1 - e^2\sin^2\phi)^{1/2}} \tag{13}$$

are the radius of curvature and the radius of curvature in prime vertical, respectively.[23] In Eqs. (1) through (7), ϕ is geographic latitude; λ is longitude, east of Greenwich being positive; r is ocean depth, downward positive; α is azimuth, measured clockwise from north; θ is grazing angle; a is the semimajor radius of the reference ellipsoid; and e is the eccentricity of the ellipsoid. Apart from these ray equations, we also use the following equation

$$\frac{dt}{ds} = \frac{1}{C}, \tag{14}$$

to compute travel time, and use the range equation

$$\frac{dR}{ds} = \cos\theta\sqrt{\left(\frac{\mu}{\mu - r}\cos\alpha\right)^2 + \left(\frac{\nu}{\nu - r}\sin\alpha\right)^2} \tag{15}$$

to estimate propagation range. The derivation of equation (15) has previously been presented in Ref.(17,19).

These equations are numerically integrated by using the fourth-order Runger-Kutta method with adaptive step size control,[24] the same as that in our previous work. The calculation accuracy is controlled by specifying a maximum fractional error (10^{-6}) in any single integration step. Sound speed is estimated using the model described in last section. An eigenray is constructed in the following way. First, we specify a launch grazing angle (θ_l) and search for the launch azimuth (α_l) that drives the ray to pass within a given error tolerance for both the latitude and the longitude of the receiver. Successive Shooting method[25] is used for the searching process. Then, we change θ_l and again search for a corresponding α_l. The searching process terminates if a ray passes within the given tolerances for the receiver's coordinates (ϕ_r, λ_r, r_r). The locations of the source and the receiver in this calculation are listed in Table 3. These data are obtained from the published references.[26,27] The receiver's parameters are those of hydrophone 23 located south of the Ascension Island.[27]

Chaos is measured by using Lyapunov exponent. Any chaotic system must have at least one positive Lyapunov exponent, and the magnitude of the exponent is a measure of chaoticity. In the following, we follow Wolf et al.'s definition. The *i*th one-dimensional Lyapunov exponent is defined as[28]

$$\lambda_i = \lim_{t\to\infty} \frac{1}{t} \log_2 \frac{p_i(t)}{p_i(0)}, \tag{16}$$

where p is the length of the ellipsoidal principle axis, and λ_i are ordered from the largest to the smallest. Wolf et al.'s method is used to estimate the Lyapunov exponent, and

their published FORTRAN code[28] is adapted for the calculations in this work. Along a ray path, we numerically integrate the variational equations given in Ref. (17), and then use Wolf et al.'s algorithm to estimate p in Eq. (16) and compute Lyapunov exponents. The magnitude of the largest Lyapunov exponent of an eigenray is used to quantify chaos.

3.2 Chaoticity

Figure 4 shows the vertical ray paths of eigenrays constructed using the smoothed sound speed. The corresponding ray parameters are listed in Table 4. Now we quantify chaoticity using the magnitude of the largest Lyapunov exponent of an eigenray. Using the method described in section 3.1, we estimate the Lyapunov exponents for all the eigenrays in Fig. 4. The largest Lyapunov exponent for each eigenray is given in Table 5. For comparison, Table 6 gives the largest Lyapunov exponent for the eigenrays computed using the original NODC data in our previous work (17,19).

Comparing Table 5 with Table 6, we can see that the eigenrays constructed using the smoothed sound speed have apparently smaller Lyapunov exponents than those computed using the original NODC sound speed data. This suggests that using the smoothed sound speed significantly reduced chaoticity. This is consistent with our hypothesis.

We can see from Table 6 that the near-axial ray paths (indicated by small identification number) had larger Lyapunov exponents. This is because that these rays were constructed using the original NODC data that have large fluctuation near the

channel axis (see Fig. 1). In Table 5, however, the near-axial rays have smaller Lyapunov exponents, because these rays are computed using the smoothed sound speed that ignores the large fluctuation in the upper ocean. Comparison between Table 5 and Table 6 suggests that the large fluctuation in the upper ocean is a main cause for the chaos in ray tracing and the smoothed sound speed reduces chaoticity by ignoring this fluctuation.

3.3 Predictability

We have just shown that the chaoticity was significantly reduced by using the smoothed sound speed. As a result, the predictability will be significantly improved, as shown in this section.

Recall that in our previous work (17,19), we used original NODC sound speed data to construct the eigenrays between Heard Island and Ascension Island. The prediction accuracy was typically less than 0.005 degree in the receiver's longitude, and less than 1 km in the receiver's depth.

Compared with this result, the prediction accuracy of this work was significantly improved. This can be seen from Table 4. From this Table, we can see that the first four eigenrays had the error of less than 0.000005 degree in the receiver's longitude, and less than 0.0005 km in the receiver's depth. Although eigenray 5 through 7 had relatively large errors. The prediction accuracy of these rays was still better than that of our previous result.

4. Summary and Discussions

The objective of this report is to investigate the feasibility of using smoothed sound speed to reduce chaoticity in acoustic ray tracing in the ocean. This is done by (1) fitting the NODC measured sound speed data to Munk's model, (2) performing ray tracing with the model-produced sound speed, and (3) comparing chaoticity with that previously produced using original NODC data. Numerical results show that

1. Chaoticity was significantly reduced by using the smoothed sound speed and consequently, the predictability was greatly improved.

2. Large fluctuation of sound speed in the upper ocean is a main cause for the chaos in acoustic ray tracing in the ocean.

Now we have a question: Did we lose the correctness of the ray tracing while enjoying the greatly improved predictability? Note that we used a model to smooth the NODC data. The model's output is just an averaged SSP for a given latitude. This is an approximation. There must be some discrepancy between the result calculated using the original NODC data and the smoothed data. To examine the correctness of the ray tracing with the smoothed sound speed, let us compare the results with those computed using the original NODC data.

First, let us compare the ray paths. According to our previous results (17,19), the vertical paths started in a shallow sound channel near Heard Island. This pattern persists along a distance of about 3000 km. Then a transition began from the shallow channel to a deep channel. The rays entered the deep channel at the propagation range of about 4000 km, and finally reached Ascension Island. This is consistent with the ray paths constructed using the smoothed sound speed (see Fig. 4).

Then, let us compare the travel times. The largest travel time computed using the smoothed sound speed was about 6248 s (see Table 4), while that produced using the original NODC sound speed data was about 6258 s. There was 10-second discrepancy between the two results. In other words, using the smoothed sound speed to approximate the original NODC data led to a relative error of 0.16% (10/6258) in ray tracing. This small error might be acceptable for such a long-range (9223 km) sound propagation. On the other hand, it was impossible to get an accurate 3-D eigenray using the original NODC data as mentioned in our previous work. Using the smoothed sound speed made it possible, however.

Acknowledgments

We acknowledge the funding from the Office of Naval Research (Grant N00014-97-1-0518). The sound speed data are provided by the National Oceanographic Data Center.

References

[1] D. Kaplan, and L. Glass, Understanding Nonlinear Dynamics (Springer-Verlag, New York, 1995) p. 27.

[2] Palmer, D. R., Brown, M. G., Tappert, F. D., and Bezdek, H. F., "Classical chaos in nonseparable wave propagation problems," *Geophys. Res. Lett.* **15**, 569-572 (1988).

[3] Abdullaev, S. S., and Zaslavskii. G. M., "Fractals and ray dynamics in a longitudinally inhomogeneous medium," **34**, 334-336 (1989).

[4] Tappert, F. D., Brown, M. G., and Goni, G., "Weak chaos in an area-preserving mapping for sound ray propagation," *Phys. Lett.* **A 153**, 181-185 (1991).

[5] Brown, M. G., Tappert, F. D., and Goni, G., "An investigation of sound ray dynamics in the ocean volume using an area preserve mapping," *Wave Motion* **14**, 93-99 (1991).

[6] Brown, M. G., Tappert, F. D., Goni, G., and Smith, K. B., "Chaos in underwater acoustics," in *Ocean Variability and Acoustic Propagation,* edited by J. Potter and A. Warn-Varnas (Kluwer Academic, Dordrecht), pp. 139-160 (1991).

[7] Smith, K. B., Brown, M. G., and Tappert, F. D., "Ray chaos in underwater acoustics," *J. Acoust. Soc. Am.* **91**, 1939-1949 (1992).

[8] Smith, K. B., Brown, M. G., and Tappert, F. D., "Acoustic ray chaos induced by mesoscale ocean structure," *J. Acoust. Soc. Am.* **91**, 1950-1959 (1992).

[9] Yan, J., "Ray chaos in underwater acoustics in view of local instability," *J. Acoust. Soc. Am.* **94**, 2739-2745 (1993).

[10] M. D. Collins, and W. A. Kuperman, "Overcoming ray chaos," J. Acoust. Soc. Am. **95**, 3167-3170 (1994).

[11] Tappert, F. D., and Tang, X., "Ray chaos and eigenrays," *J. Acoust. Soc. Am.* **99**, 185-195 (1996).

[12] Munk, W. H., O'Reilly, W. C., and Reid J. L., "Australia-Bermuda sound transmission experiment (1960) revisited," J. Phy. Oceanogr. 18, 1876-1898 (1988).

[13] Heaney, K. D., Kuperman, W. A., and McDonald, B. E., "Perth-Bermuda sound propagation (1960): adiabatic mode interpretation," J. Acoust. Soc. Am., 90, 2586-2594 (1991).

[14] Jones, R. M., Riley, J. P., Georges, T. M., "HARPO—A versatile three-dimensional Hamiltonian ray-tracing program for acoustic waves in an ocean with irregular bottom," NOAA Report, Environmental Research Laboratory, Boulder, CO (1986).

[15] Yan, J., and Yen, K., "A derivation of three-dimensional ray equations in ellipsoidal coordinates," *J. Acoust. Soc. Am.*, **97**, 1538-1544 (1995).

[16] Yan, J., and Yen, K. K., "Ray chaos of underwater sound in long-range propagation," in *Chaotic, Fractal, and Nonlinear Signal Processing*, edited by Richard A. Katz (AIP Press, New York, 1995), pp. 231-238.

[17] K. Yen, and J. Yan, "Investigating chaos in ocean acoustics," Florida International University Technical Report, prepared under the grant (N00014-95-10443) from the Office of Naval Resarch, January, 1997.

[18] J. Yan, and K. Yen, "Constructing three-dimensional ray paths for underwater sound from Heard Island to Ascension Island," in Computational Acoustics and Its Environmental Applications II (Computational Mechanics Publications, Southampton, UK, 1997) pp. 41-48, Eds. C. A. Brebbia et al.

[19] J. Yan, and K. Yen, "Investigating chaos in three-dimensional ray tracing," submitted to J. Acoust. Soc. Am. 1998.

[20] W. H. Munk, "Sound channel in an exponentially straitified ocean with applications to SOFAR," J. Acoust. Soc. Am. 55 (2), 220-226 (1974).

[21] P. E. Gill, and W. Murray, Numerical Methods for Constrained Optimization (Academic Press, London, 1974) pp. 208-212.

[22] S. L. S. Jacoby, and J. S. Kowalik, and J. T. Pizzo, Iterative Methods for Nonlinear Optimization Problems (Prentice-Hall, Inc., Englewood Cliffs, 1972) pp. 195-197.

[23] Bomford, G. *Geodesy*, Oxford University Press, London, 1971.

[24] Press, W. H., Flannery, B. P., Teukolsky, S. A. & Vetterling, W. T. *Numerical Recipes, The Art of Scientific Computing*, Cambridge University Press, New York, 1988.

[25] Carnahan, B. *Applied Numerical Methods*, Wiley, New York, 1969.

[26] Georges, T. M., Boden, L. R., and Palmer, D. R., "Features of the Heard Island signals received at Ascension," *J. Acoust. Soc. Am.*, **96**, 2441-2447 (1994).

[27] Palmer, D. R., Georges, T. M., Wilson, J. J., Weiner, L. D., Paisley, J. A., Mathiesen, R., Pleshek, R. R., and Mabe, R. R., "Reception at Ascension of the Heard Island feasibility test transmissions," *J. Acoust. Soc. Am.*, **96**, 2432-2440 (1994).

[28] Wolf, A., Swift, J. B., Swinney, H. L., and Vastano, J. A., "Determining Lyapunov exponents from a time series," *Physica D* **16**, 285-317 (1985).

Table 1 NODC standard depth

Depth (m)									
0	10	20	30	50	75	100	125	150	200
250	300	400	500	600	700	800	900	1000	1100
1200	1300	1400	1500	1750	2000	2500	3000	4000	5000

Table 2 Fitting NODC data to Munk's Model

Latitude (degree)	Model Parameters				Standard Deviation
	C_a	ε	z_a	B	
8S	1.483221	0.002194	0.732704	0.472351	0.00829
9S	1.482676	0.002421	0.747110	0.498450	0.00559
10S	1.482837	0.002226	0.715887	0.464047	0.00346
11S	1.482376	0.002211	0.715331	0.456252	0.00460
12S	1.483215	0.002044	0.700050	0.452106	0.00297
13S	1.482321	0.002610	0.747294	0.511343	0.00379
14S	1.481682	0.003434	0.818365	0.612715	0.00439
15S	1.481949	0.003451	0.835788	0.619859	0.00369
16S	1.482206	0.003358	0.812779	0.602596	0.00064
17S	1.482156	0.003563	0.848575	0.645464	0.00065
18S	1.481896	0.004038	0.896096	0.706073	0.00023
19S	1.482056	0.004727	0.913893	0.782972	0.00389
20S	1.482463	0.004605	0.927040	0.780659	0.00429
21S	1.482562	0.005757	0.997749	0.923985	0.00442
22S	1.482844	0.005775	0.996901	0.924338	0.00280
23S	1.482559	0.005437	0.999972	0.890491	0.00384
24S	1.482920	0.005638	0.999393	0.917236	0.00549
25S	1.483193	0.006417	0.999880	0.987625	0.00141
26S	1.481971	0.006695	0.983354	1.020320	0.00947
27S	1.482843	0.007946	1.057264	1.159711	0.00225
28S	1.482556	0.008726	1.090114	1.240750	0.00907
29S	1.481656	0.006837	1.012344	1.029022	0.00290
30S	1.482742	0.007310	1.097952	1.136131	0.00382
31S	1.484858	0.009990	1.176254	1.414319	0.00656
32S	1.484963	0.009949	1.199543	1.451312	0.00421
33S	1.484999	0.009894	1.195681	1.448759	0.00553
34S	1.484671	0.009974	1.132879	1.459401	0.00095
35S	1.484995	0.007662	1.099913	1.218559	0.01729
36S	1.484234	0.009995	1.191613	1.431734	0.01088
37S	1.482627	0.007826	1.080397	1.181853	0.00775
38S	1.488353	0.009999	1.278593	1.634727	0.03697
39S	1.487902	0.009176	1.199978	1.481553	0.03103
40S	1.485842	0.005718	1.038763	1.081195	0.02093
41S	1.481831	0.004701	0.883005	0.870412	0.00542
42S	1.482055	0.009847	0.991699	1.469271	0.02515
43S	1.480181	0.004828	0.796828	0.896648	0.01789
44S	1.477453	0.093715	0.689430	1.315256	0.00232
45S	1.474089	0.003699	0.484000	0.702803	0.00126
46S	1.471392	0.009948	0.380606	1.384595	0.00509

47S	1.467830	0.002195	0.300742	0.400003	0.00440
48S	1.464943	0.002192	0.066605	0.419463	0.00163
49S	1.462756	0.002269	0.143387	0.401664	0.00208
50S	1.460705	0.002239	0.010283	0.400460	0.00241
51S	1.457501	0.002644	0.001047	0.401966	0.00031
52S	1.460736	0.002236	0.052927	0.400119	0.00327

Table 3 Parameters of source and receiver

	Source	Receiver
Latitude (Deg)	53°22'S	8°4.2'S
Longitude (Deg)	74°30'E	14°25.2'W
Depth (km)	0.175	0.832

Table 4 Eigenray parameters

No.	Launch angles (degree)		Travel time(s)	Range (km)	Er*	Eλ**
	Grazing	Azimuth				
1	-1.425323486328125	265.6134263277054	6248.5	9222.4	0.0004	3×10^{-6}
2	-1.639988307326689	265.6392212957143	6248.5	9222.4	0.0005	6×10^{-7}
3	2.2421875	265.724887589873	6248.6	9222.4	0.0002	1×10^{-6}
4	4.091796875	265.903826713562	6248.1	9222.3	0.0004	4×10^{-6}
5	-4.2421875	265.9238282442446	6248.1	9222.3	0.001	7×10^{-4}
6	-4.60302734375	265.9766235686838	6247.7	9222.2	0.0003	1×10^{-3}
7	6.467772959697868	266.243524546997	6245.6	9222.2	0.0001	2×10^{-4}

* $E_r = |r_{end} - 0.832|$

** $E_\lambda = |\lambda_{end} - 0.000005|$.

Table 5 Lyapunov exponent of eigenrays

Eigenray No.	Largest Lyapunov exponent (1/km)
1	2.6×10^{-3}
2	2.8×10^{-3}
3	4.2×10^{-3}
4	1.7×10^{-2}
5	1.7×10^{-2}
6	1.8×10^{-2}
7	2.0×10^{-2}

Table 6 Lyapunov exponent of eigenrays computed using NODC data

Eigenray No.	Largest Lyapunov exponent (1/km)
1	1.1×10^{-1}
2	1.1×10^{-1}
3	3.8×10^{-2}
4	4.0×10^{-2}

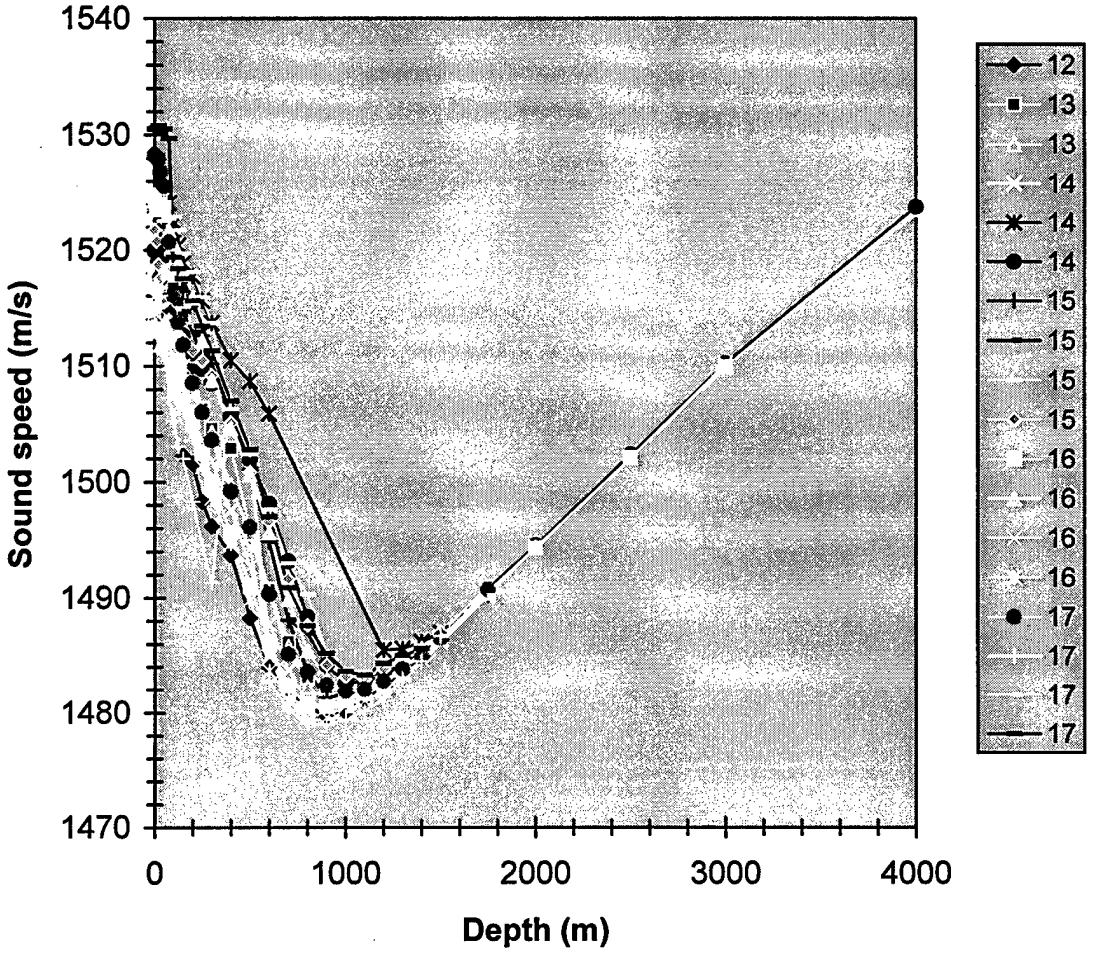

Fig. 1 NODC sound speed profiles of the Atlantic Ocean (Latitude 15 °S, Longitude from 1 °W to 13 °W). The sound speed fluctuates significantly at the upper ocean, but they are similar in shape

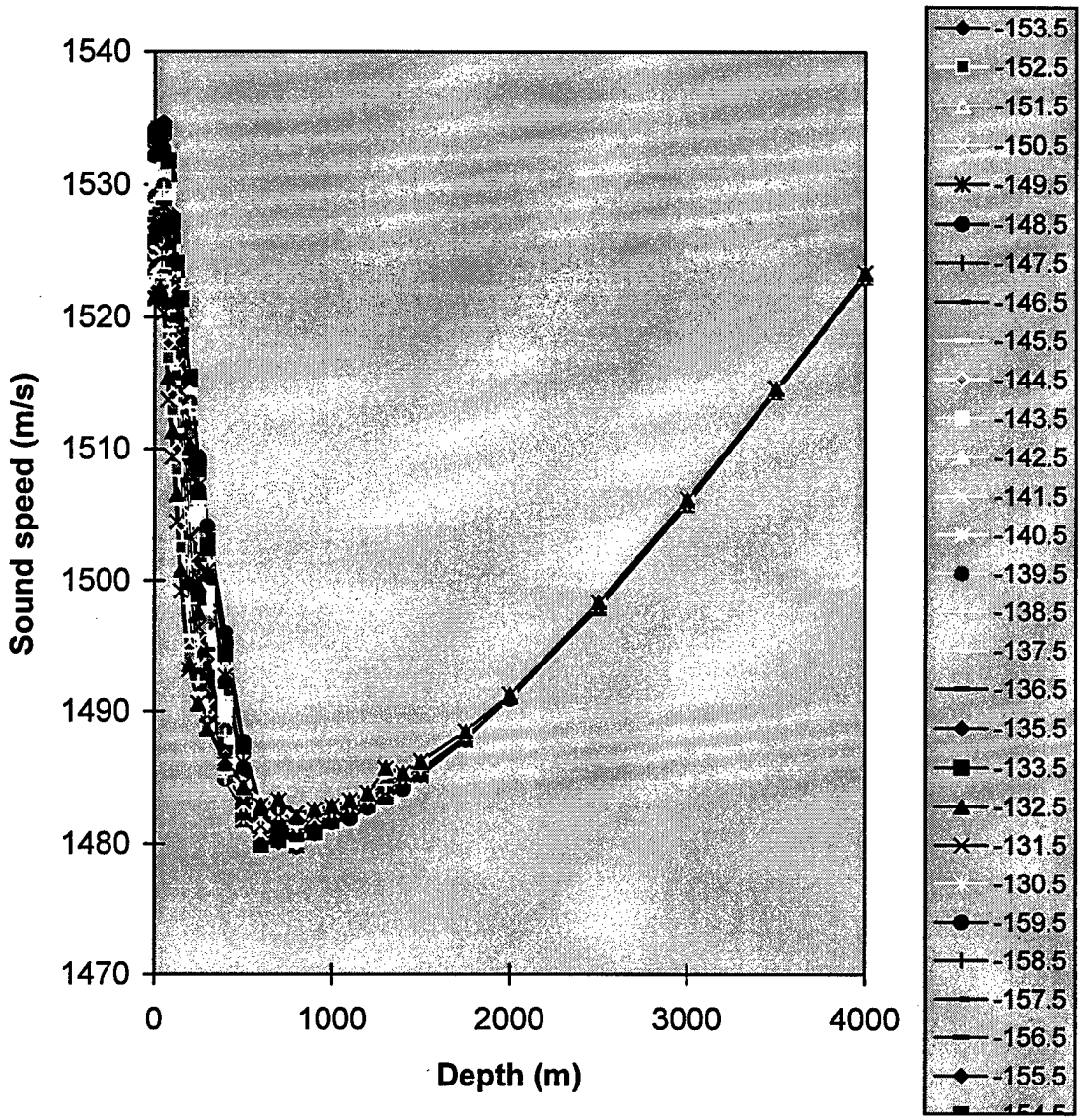

Fig. 2 Levitus sound speed profiles of Pacific Ocean (Latitude 25.5 °N, Longitude from 159.5 °W to 120.5 °W). These profiles are relatively smooth compared with the NODC data in Fig. 1

3-1 Latitude: 9 S

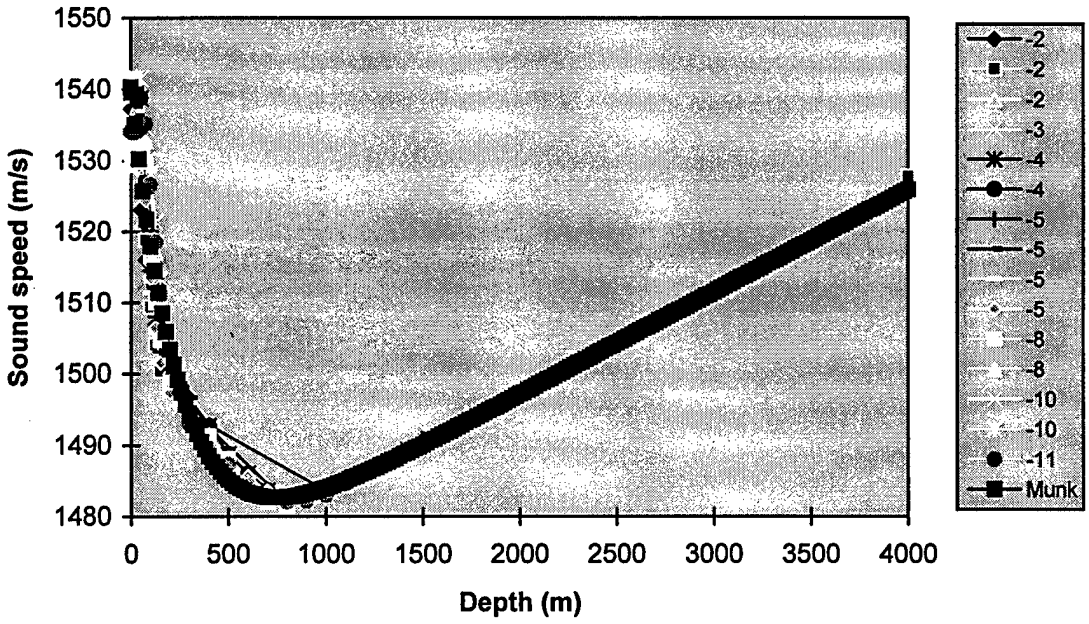

3-2 Latitude: 45S

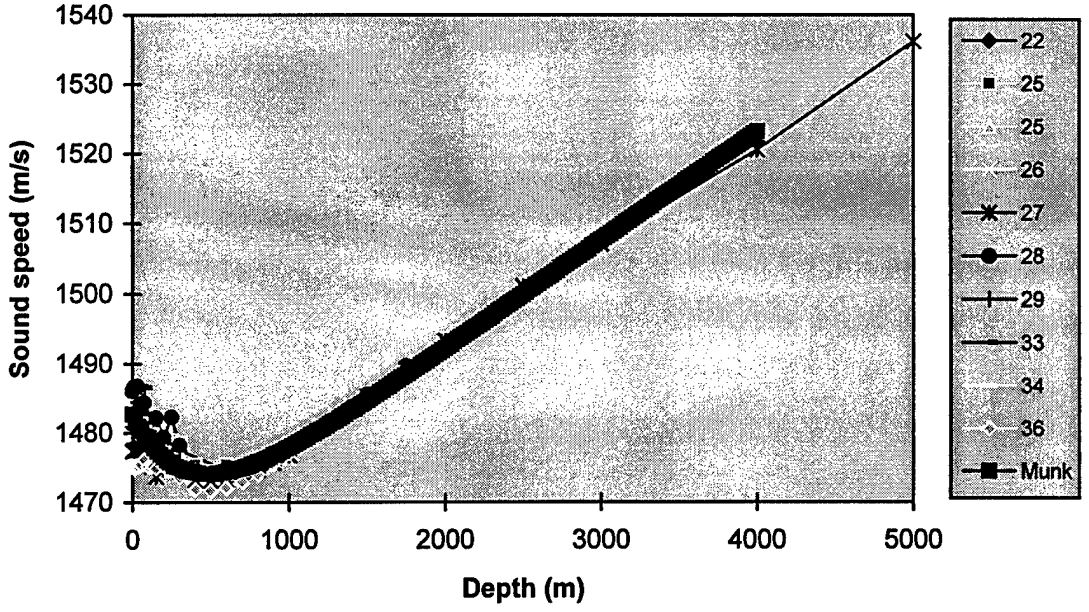

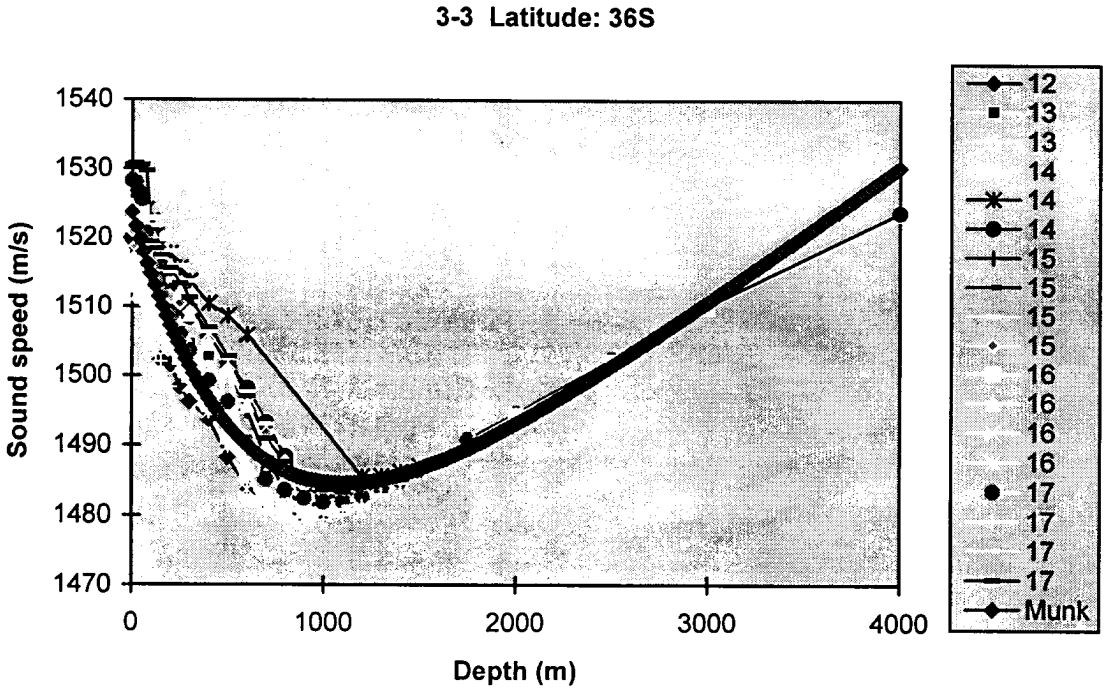

Fig. 3 Typical results of fitting NODC data to Munk's model

Eigenray 1

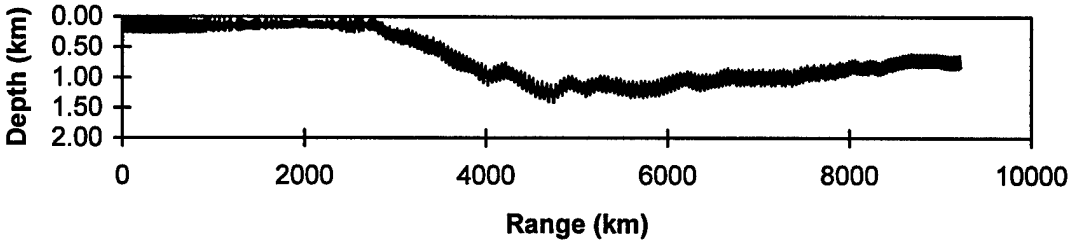

Eigenray 2

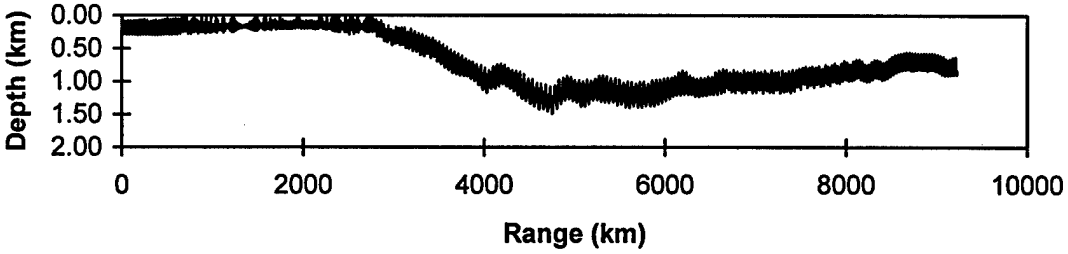

Eigenray 3

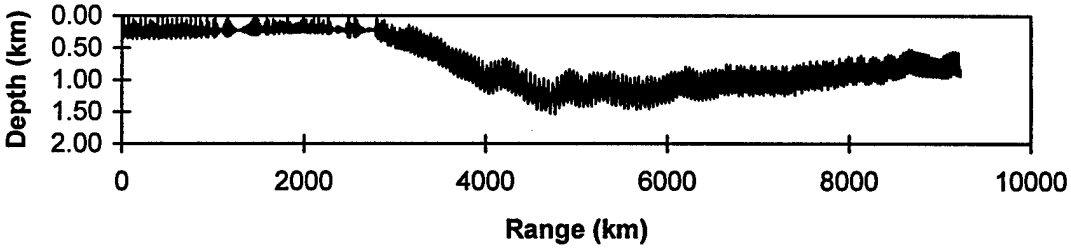

Eigenray 4

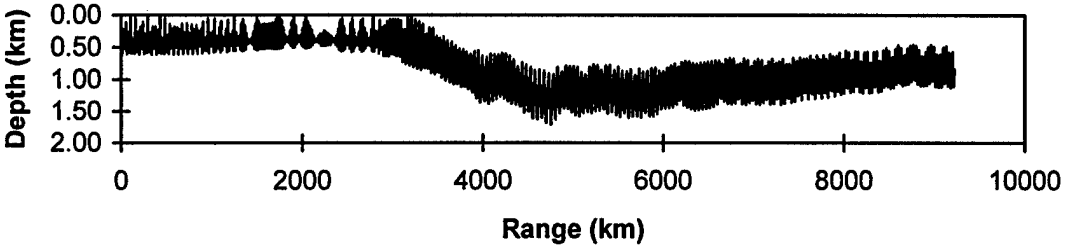

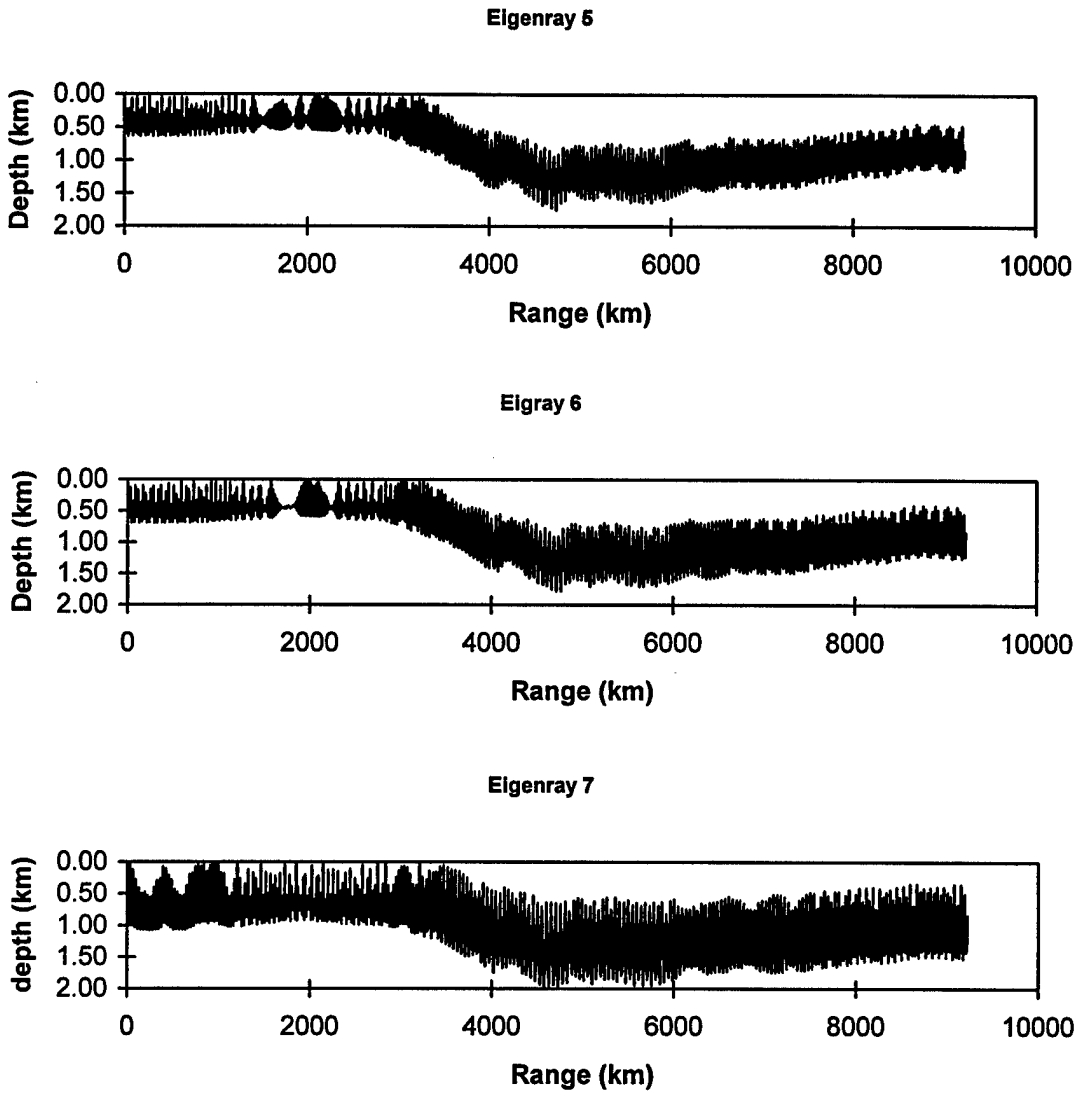

Fig. 4 Vertical ray paths of eigenrays between Heard Island and Ascension Island

Appendix

Fitting NODC sound speed data to Munk's model

In the following figures, the numbers in the legend denote longitudes, and the model output is a thick line.

Latitude: 9 S

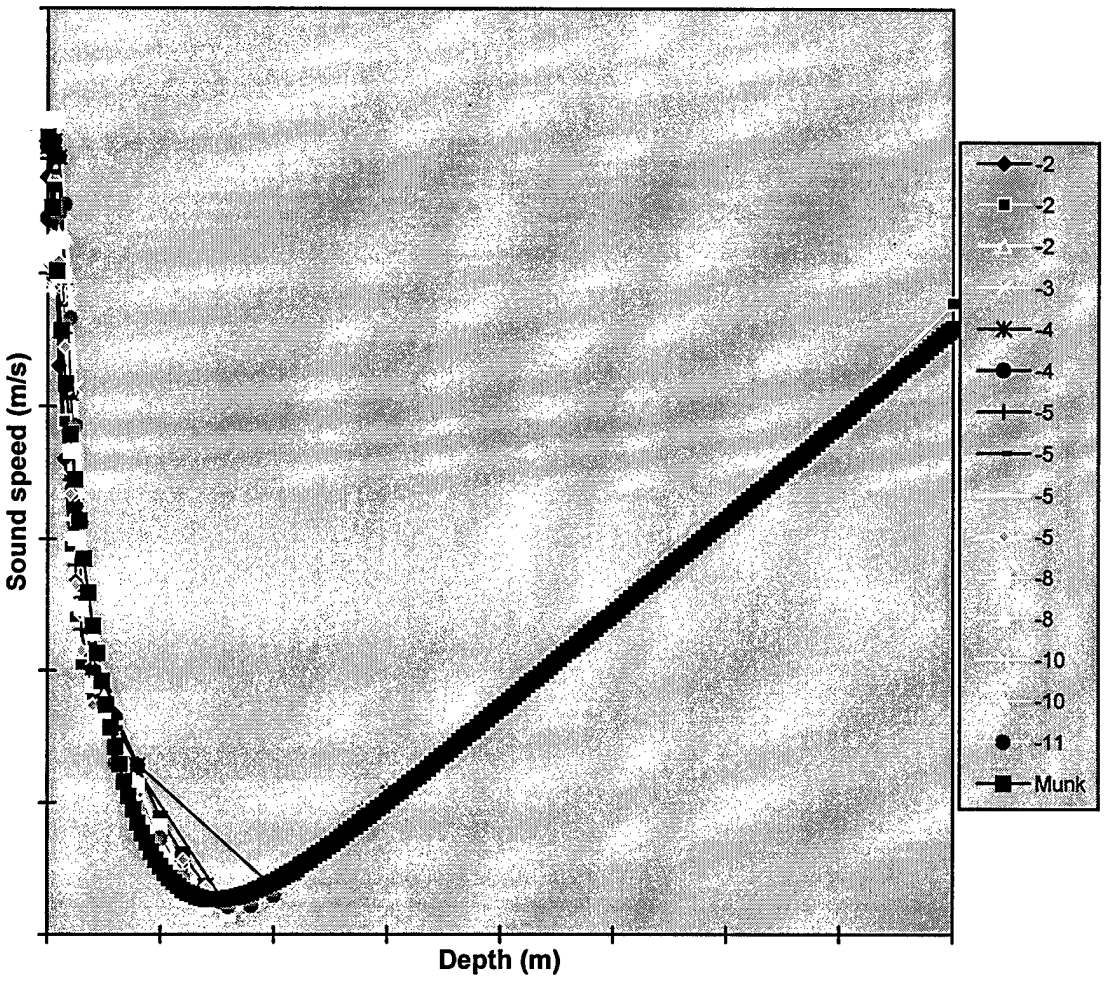

Latitude: 10 S

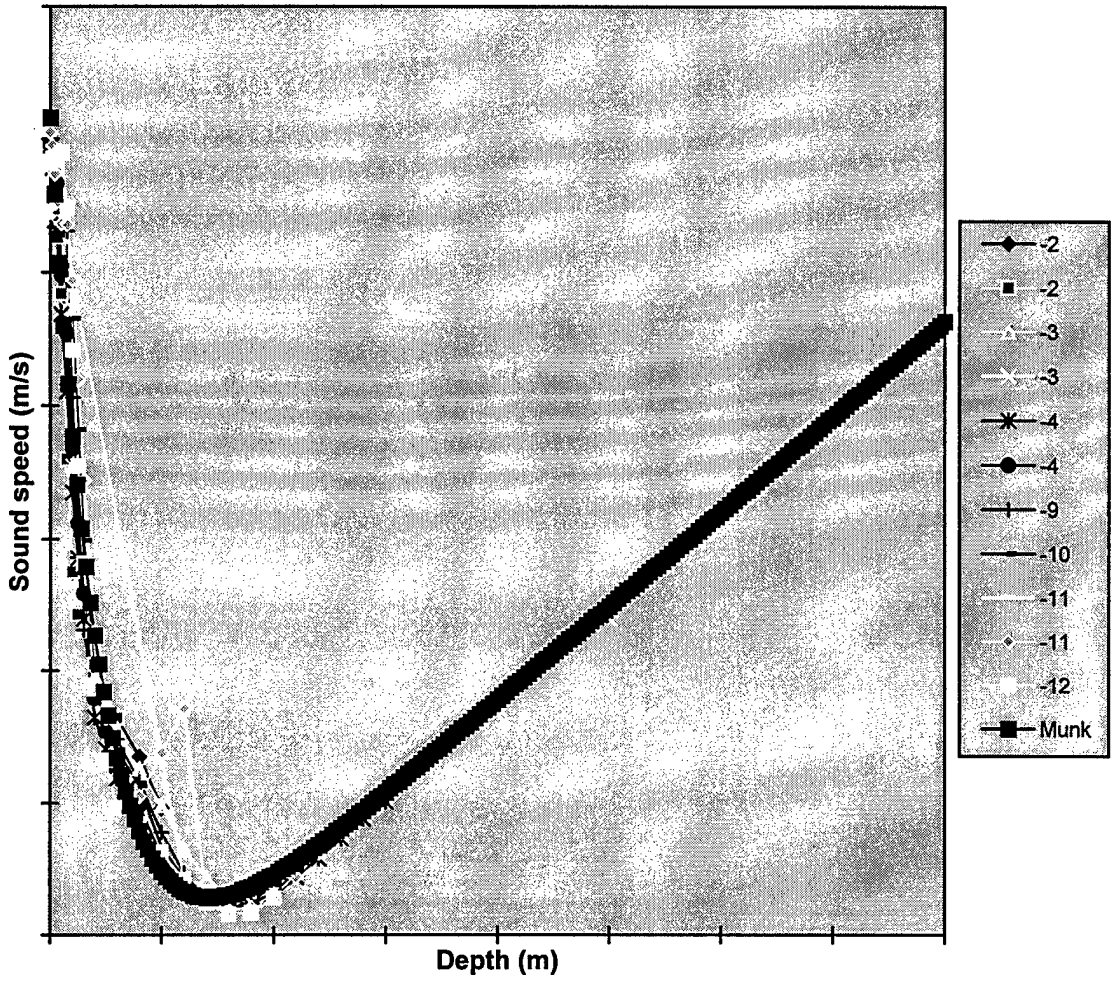

Latitude: 11 S

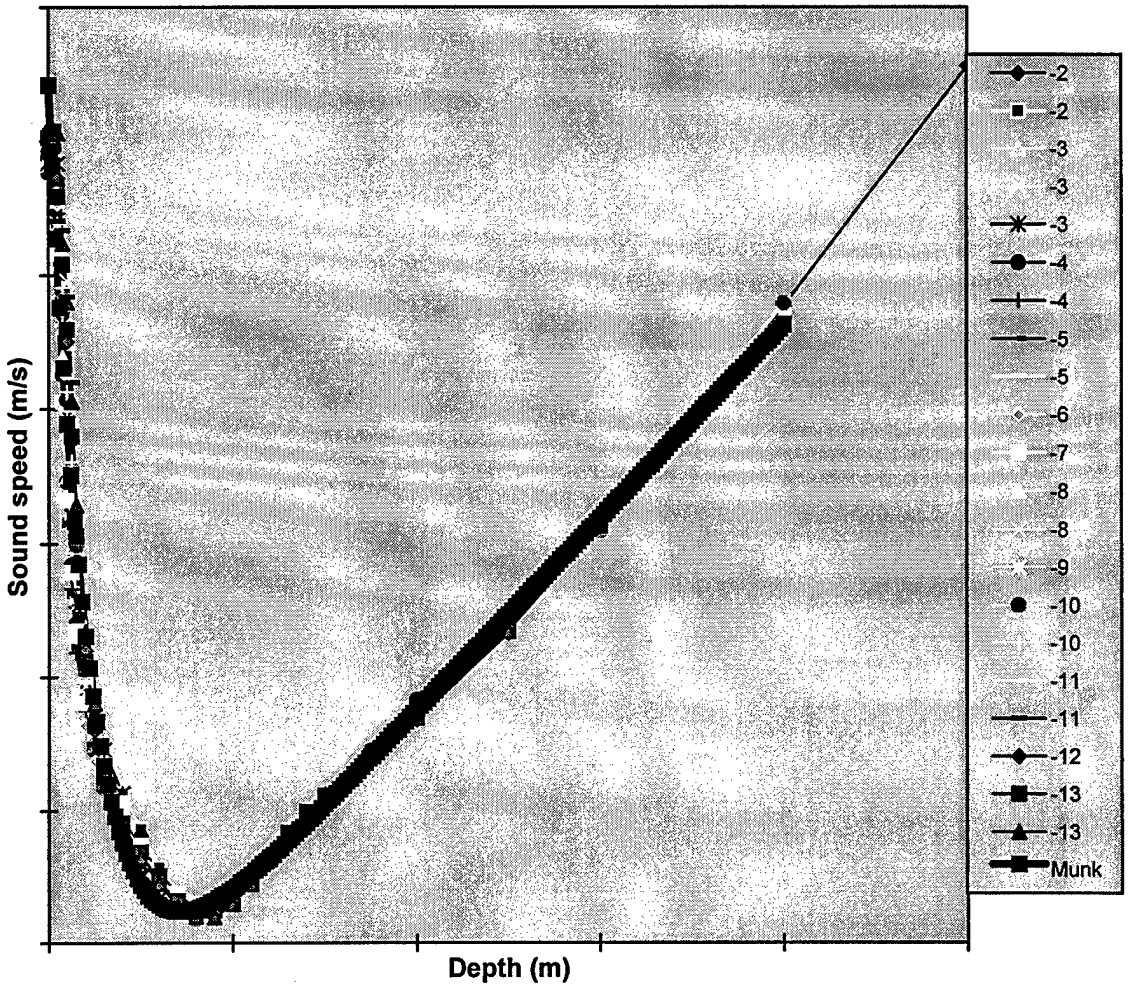

Latitude: 12 S

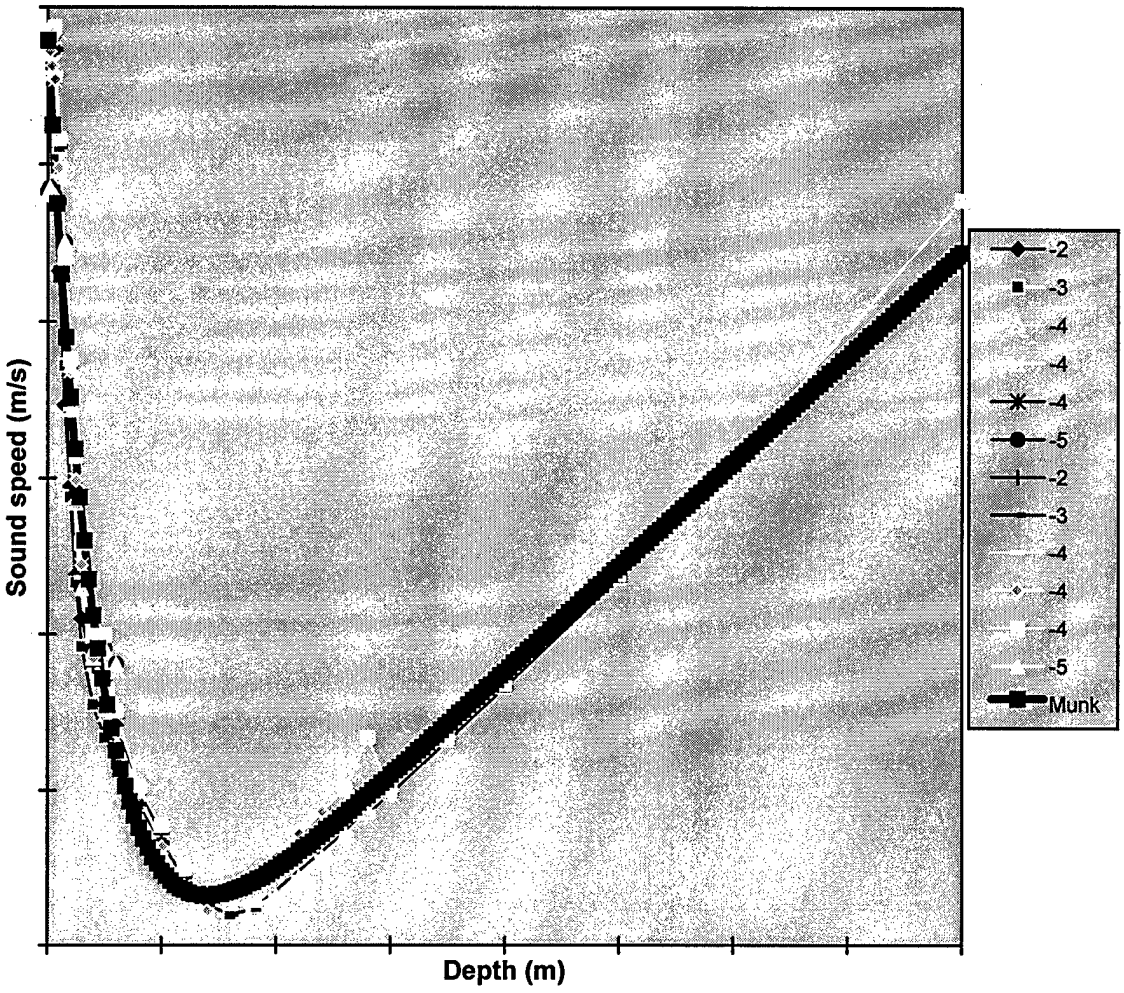

Latitude: 13 S

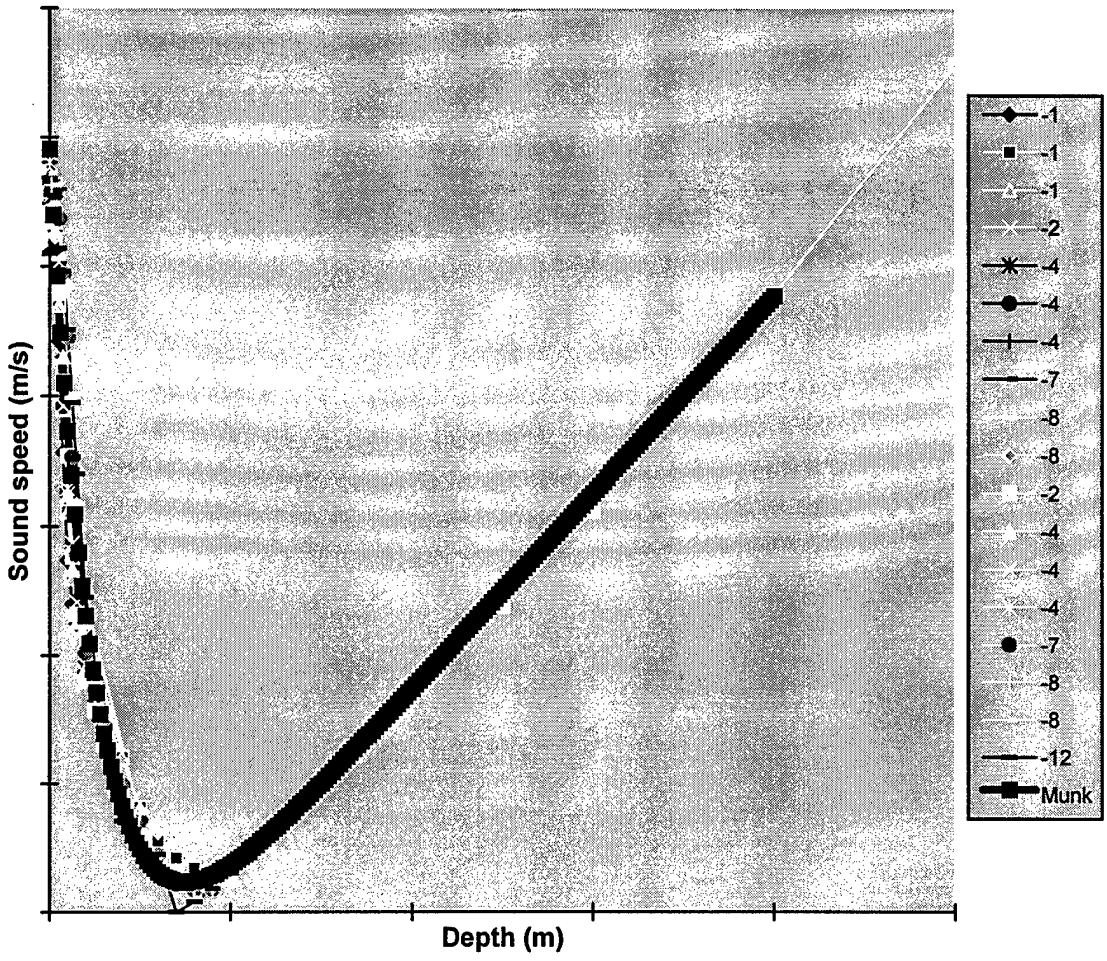

Latitude: 14 S

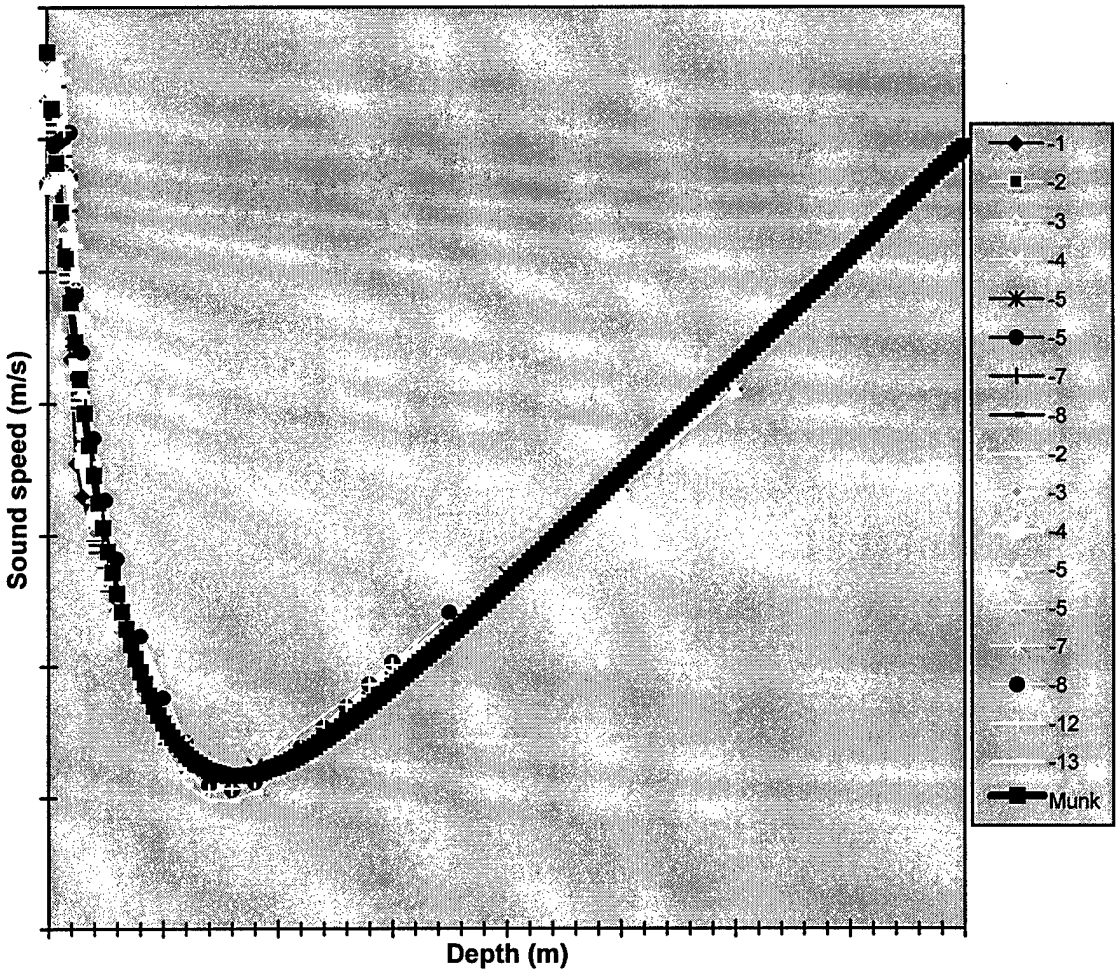

Latitude: 15 S

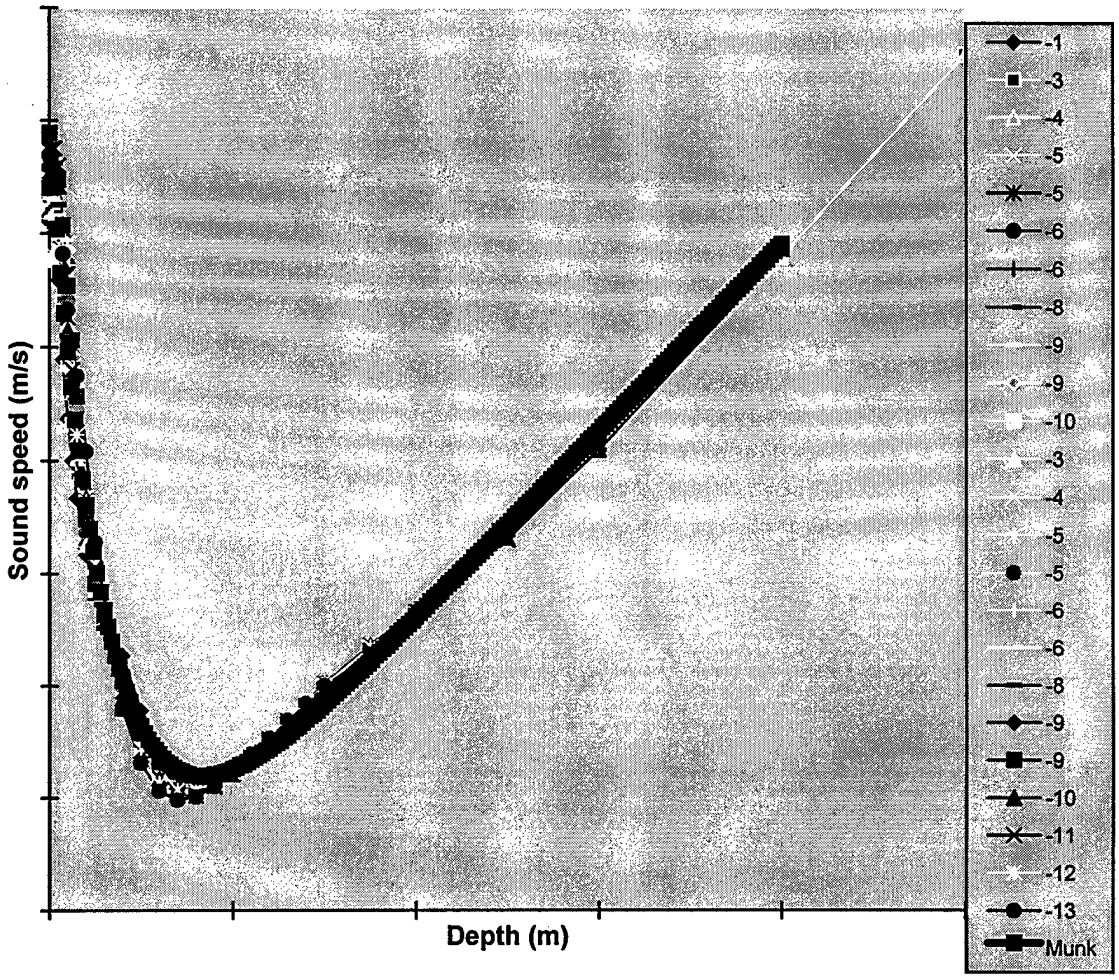

Latitude: 16 S

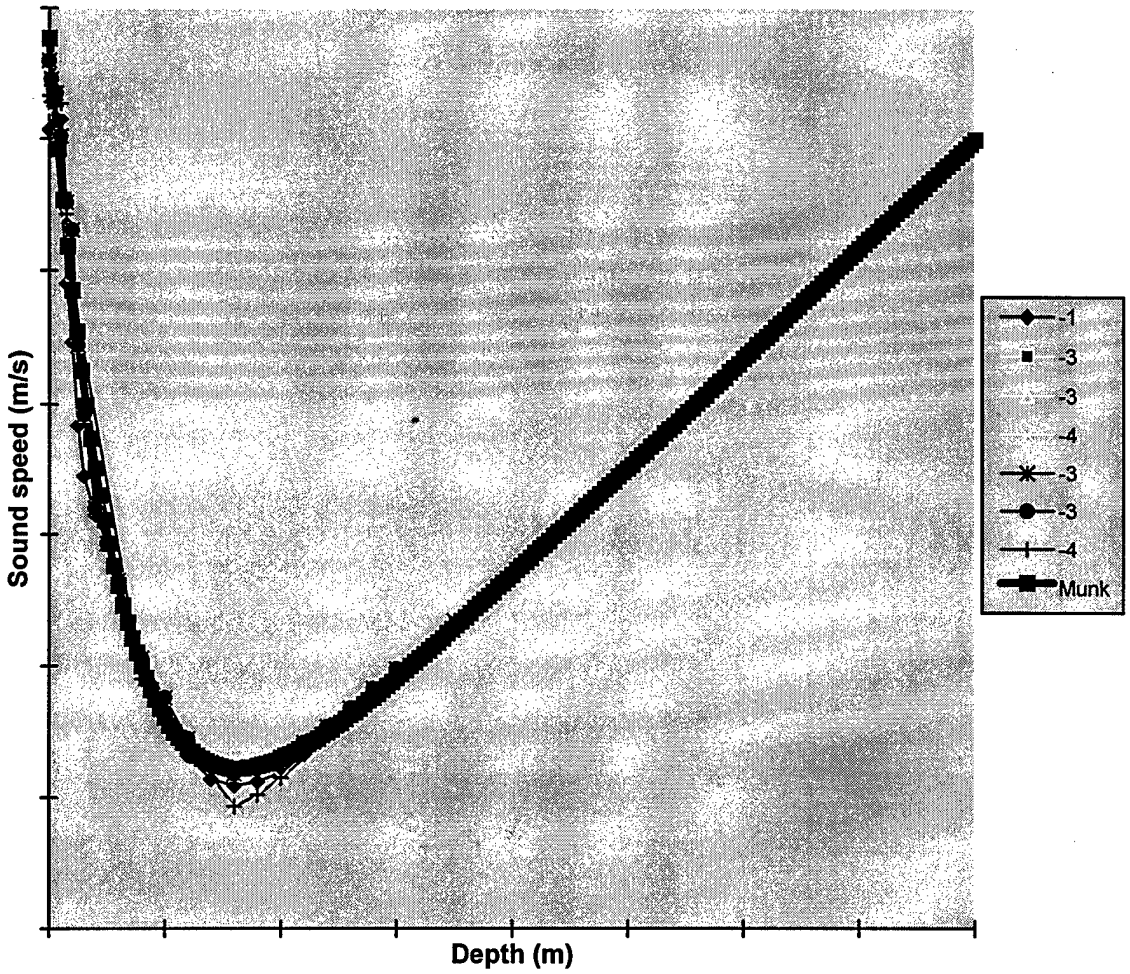

Latitude: 17S

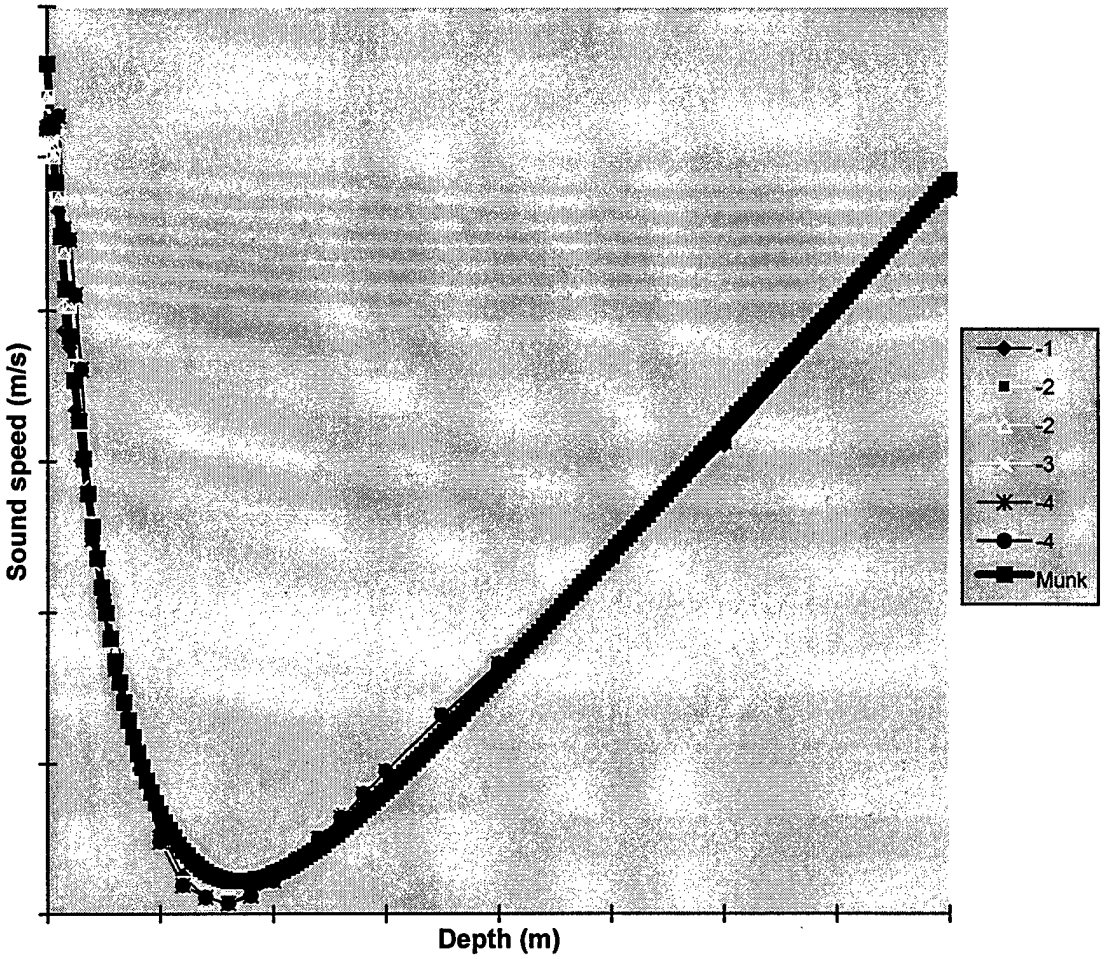

Latitude: 18 S

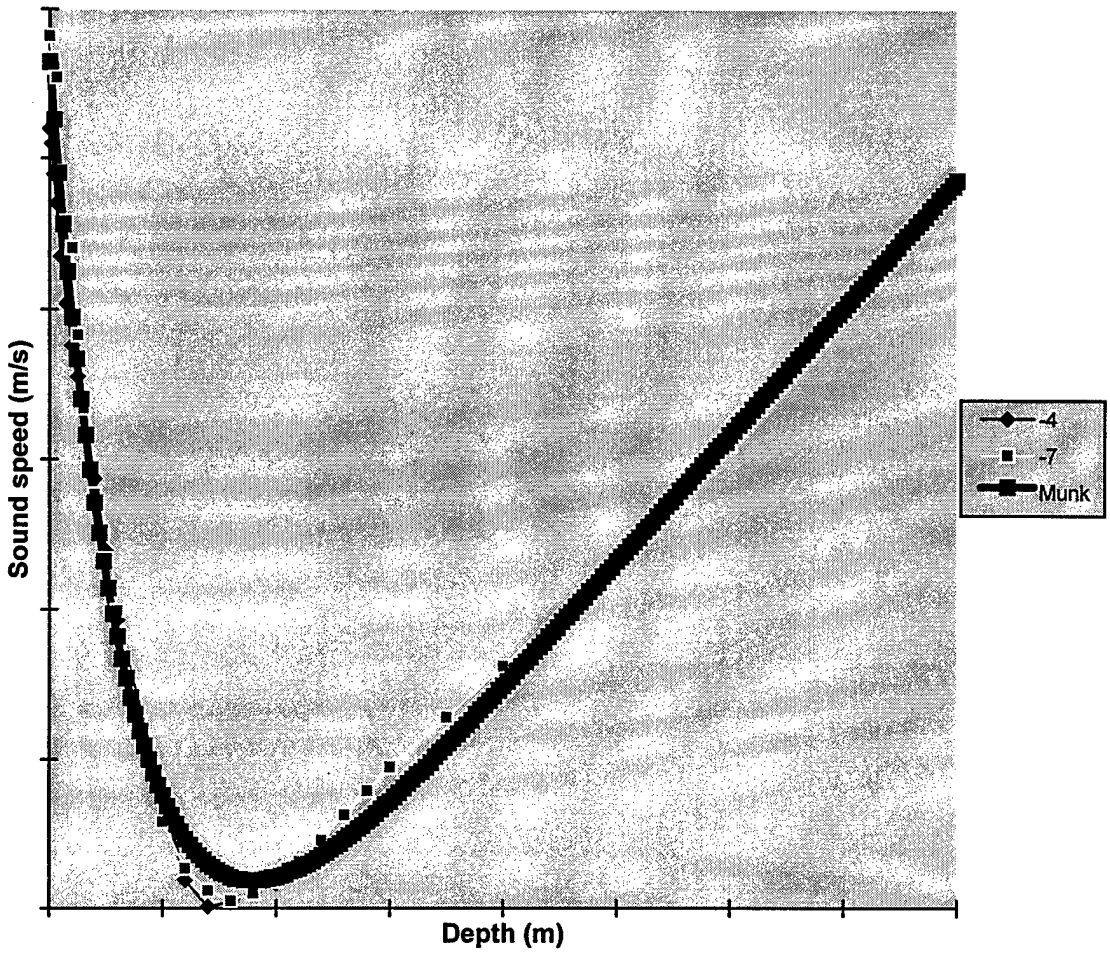

Latitude: 19S

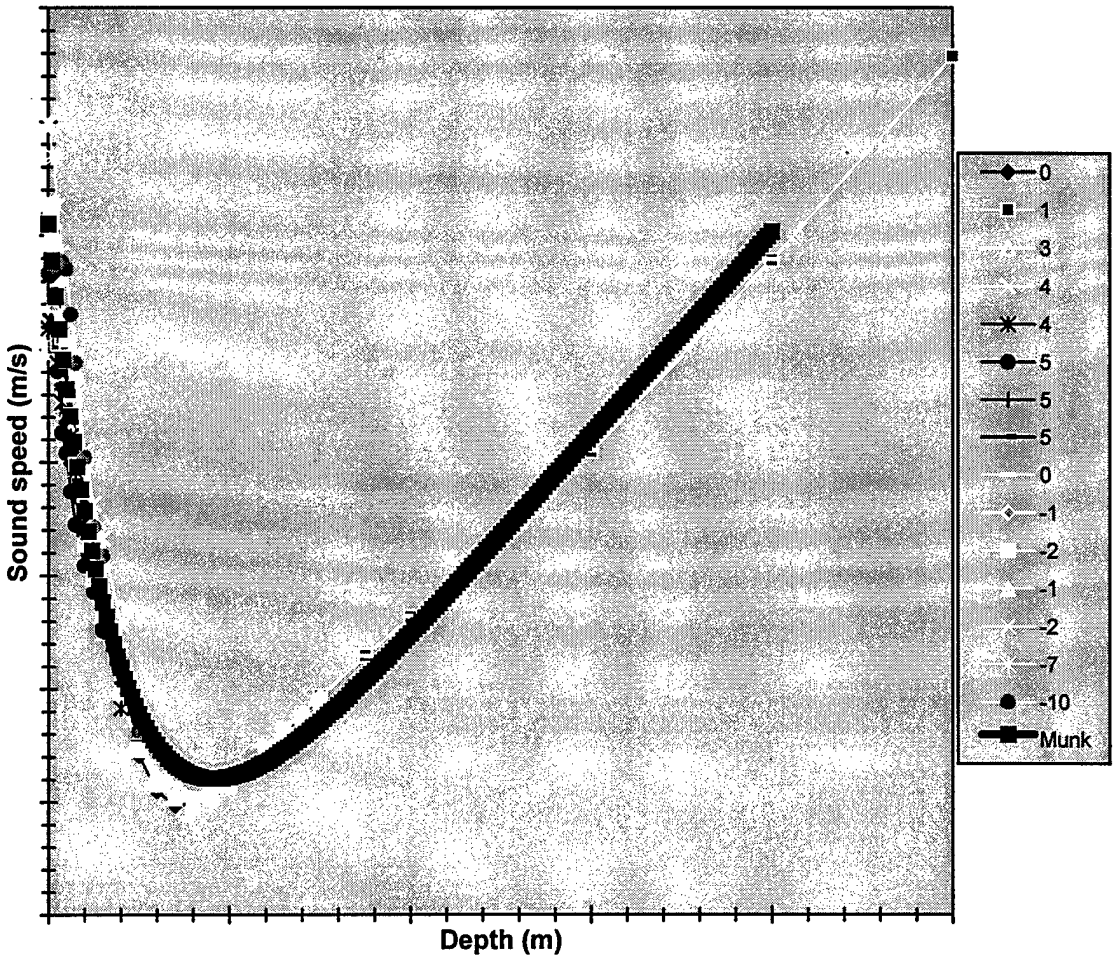

Latitude:20S

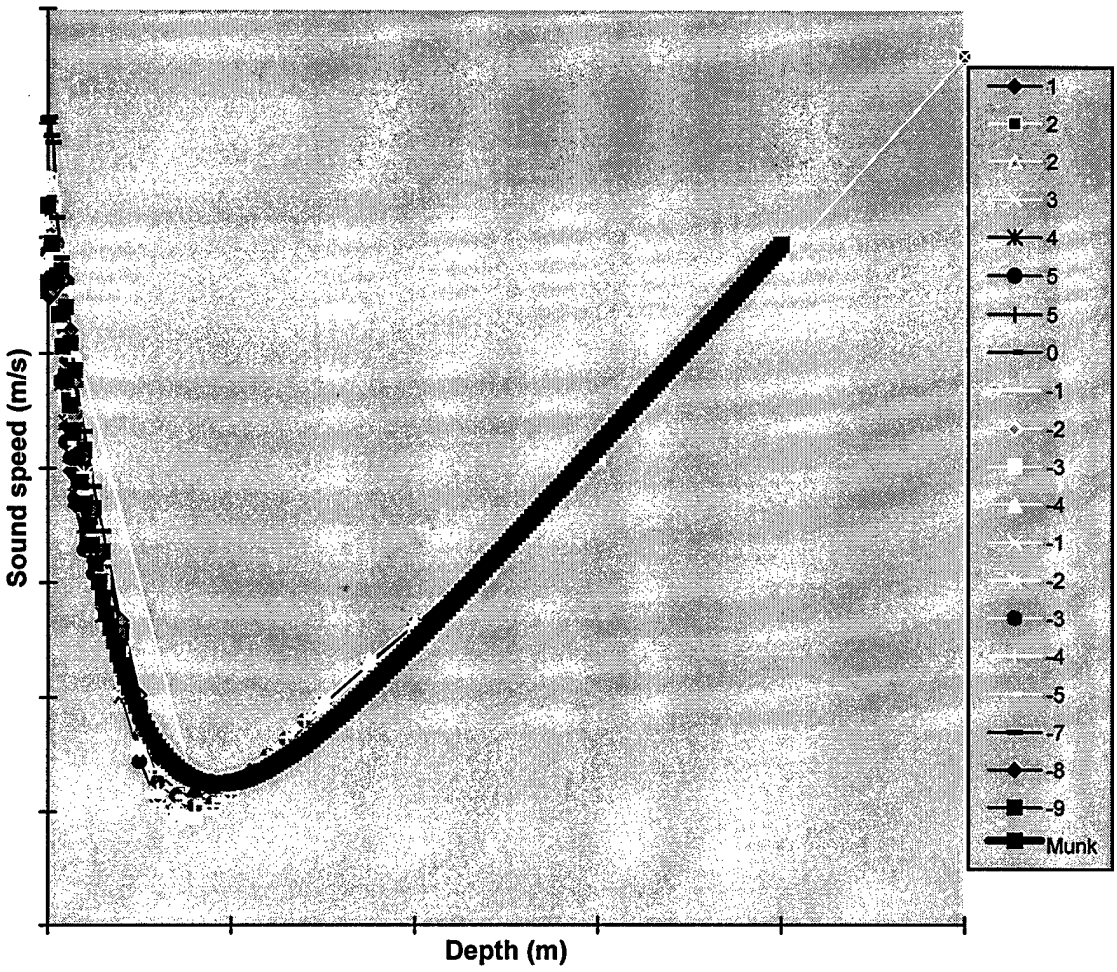

Latitude: 21 S

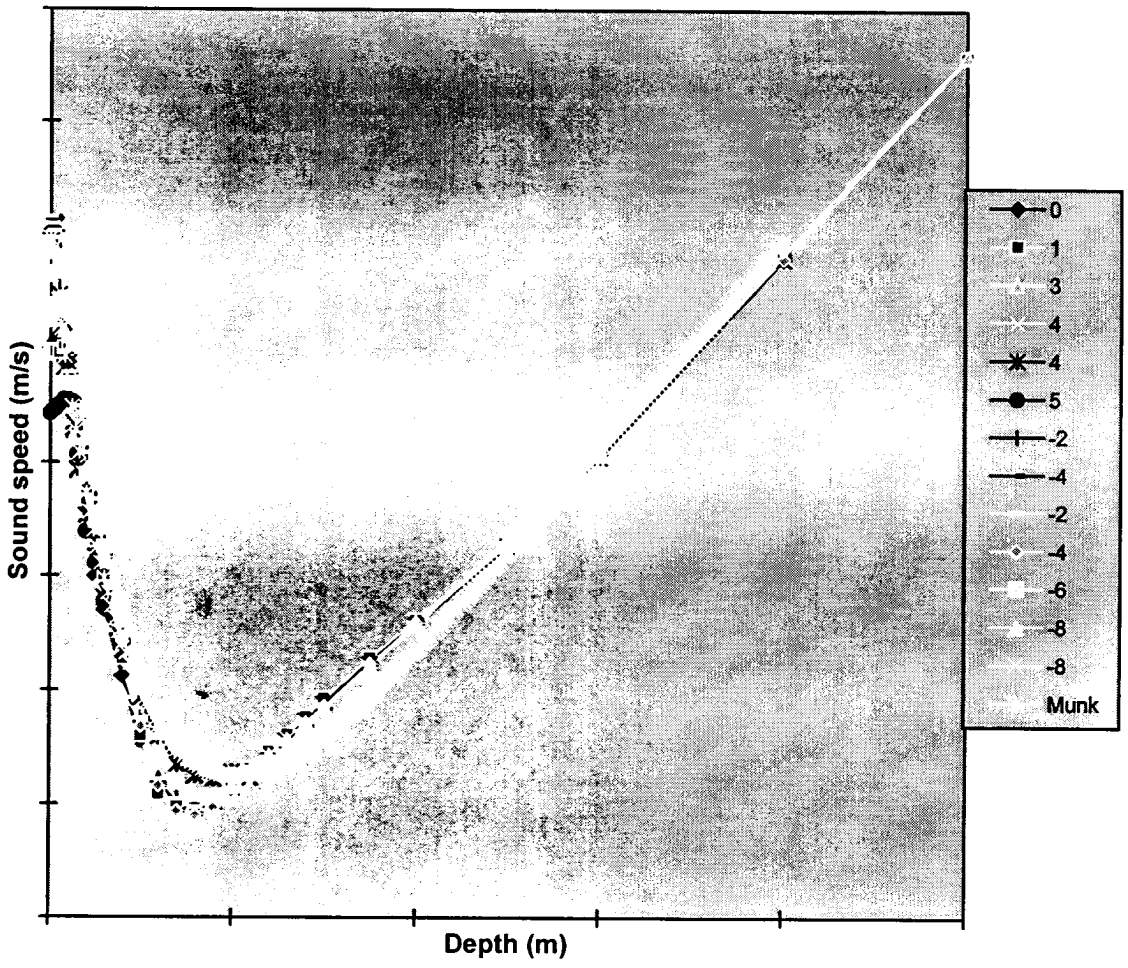

Latitude: 22 S

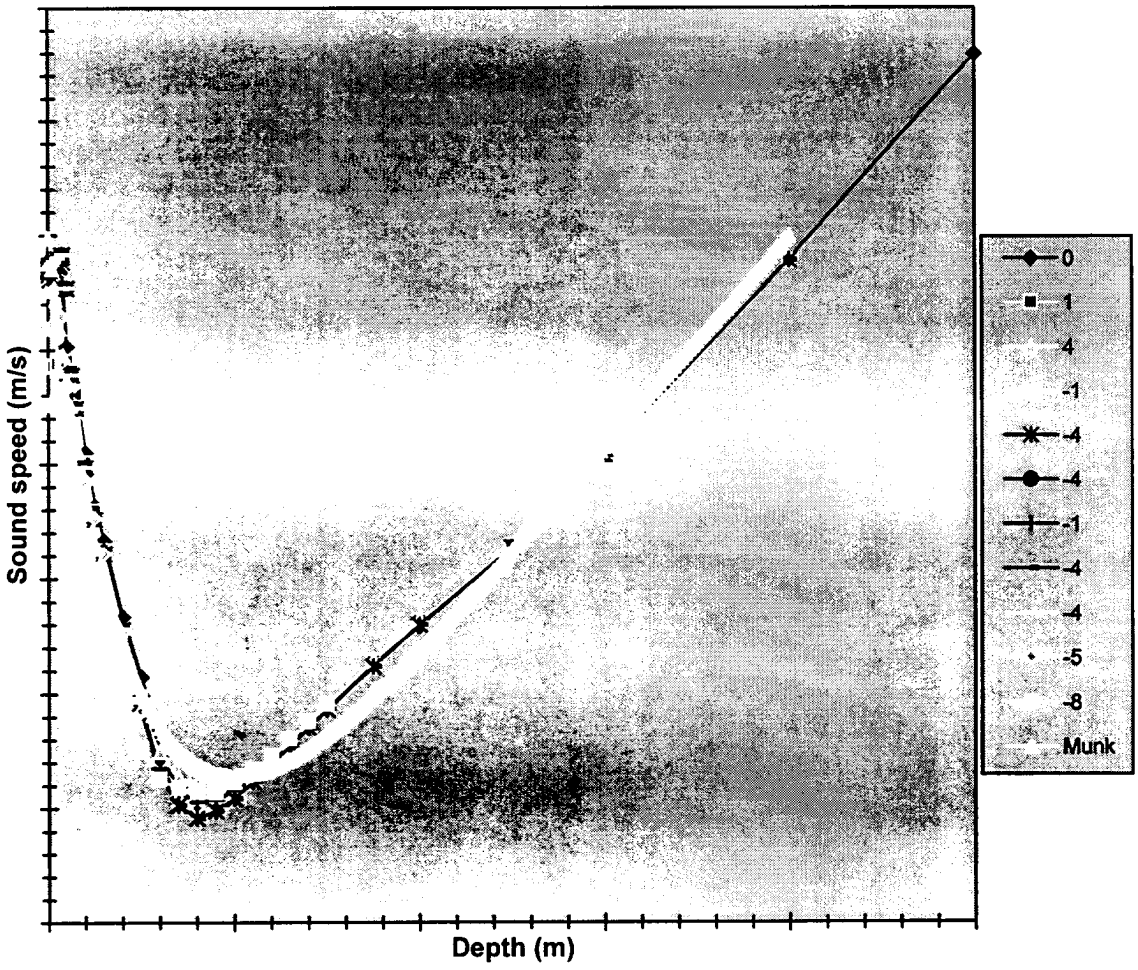

Latitude: 23 S

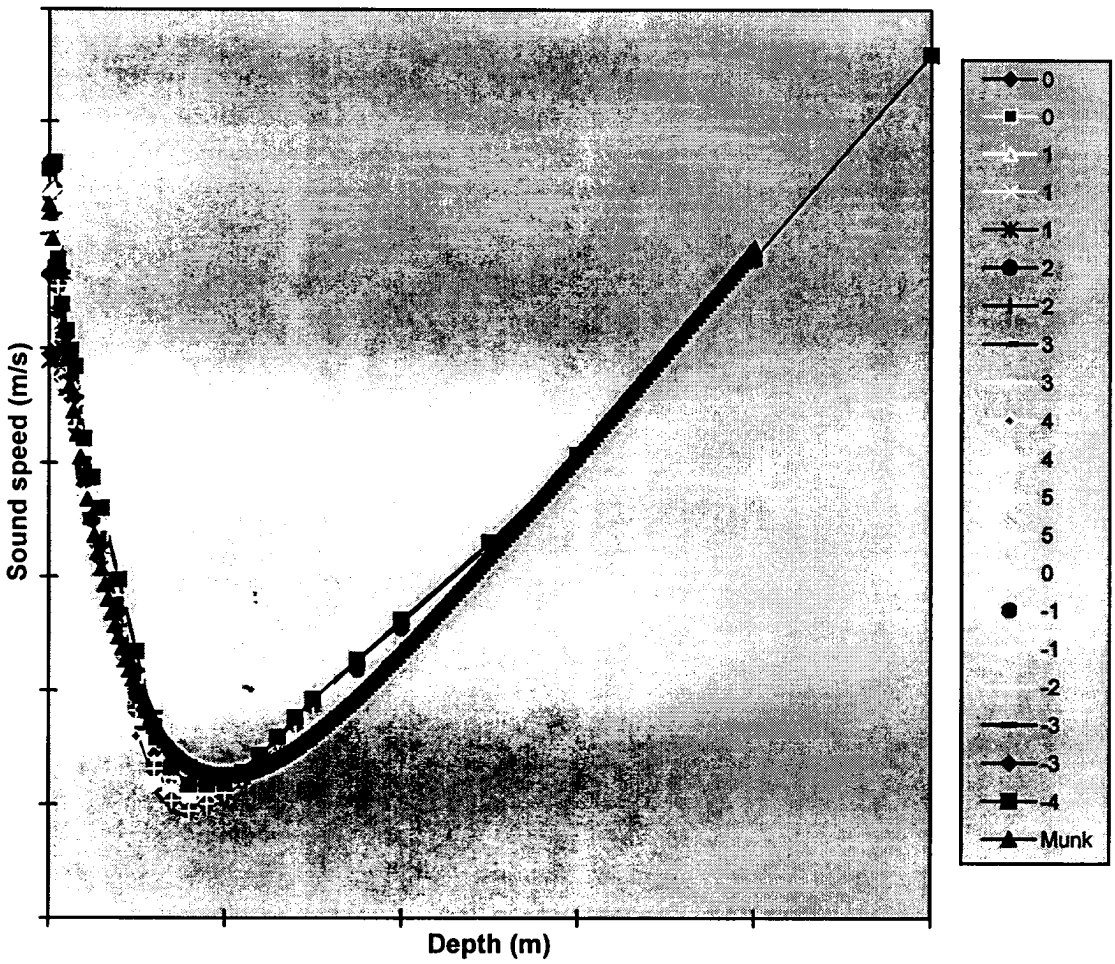

Latitude: 24S

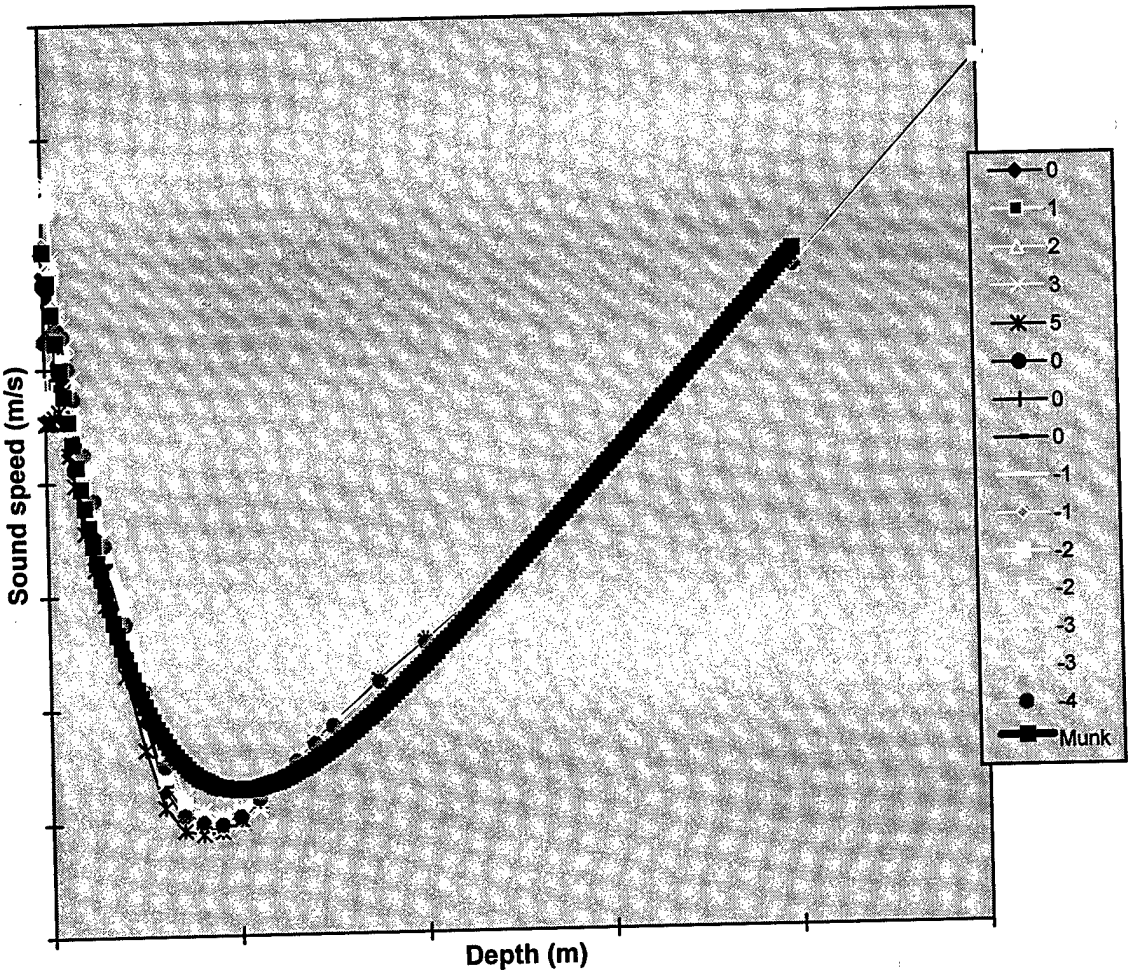

Latitude: 25 S

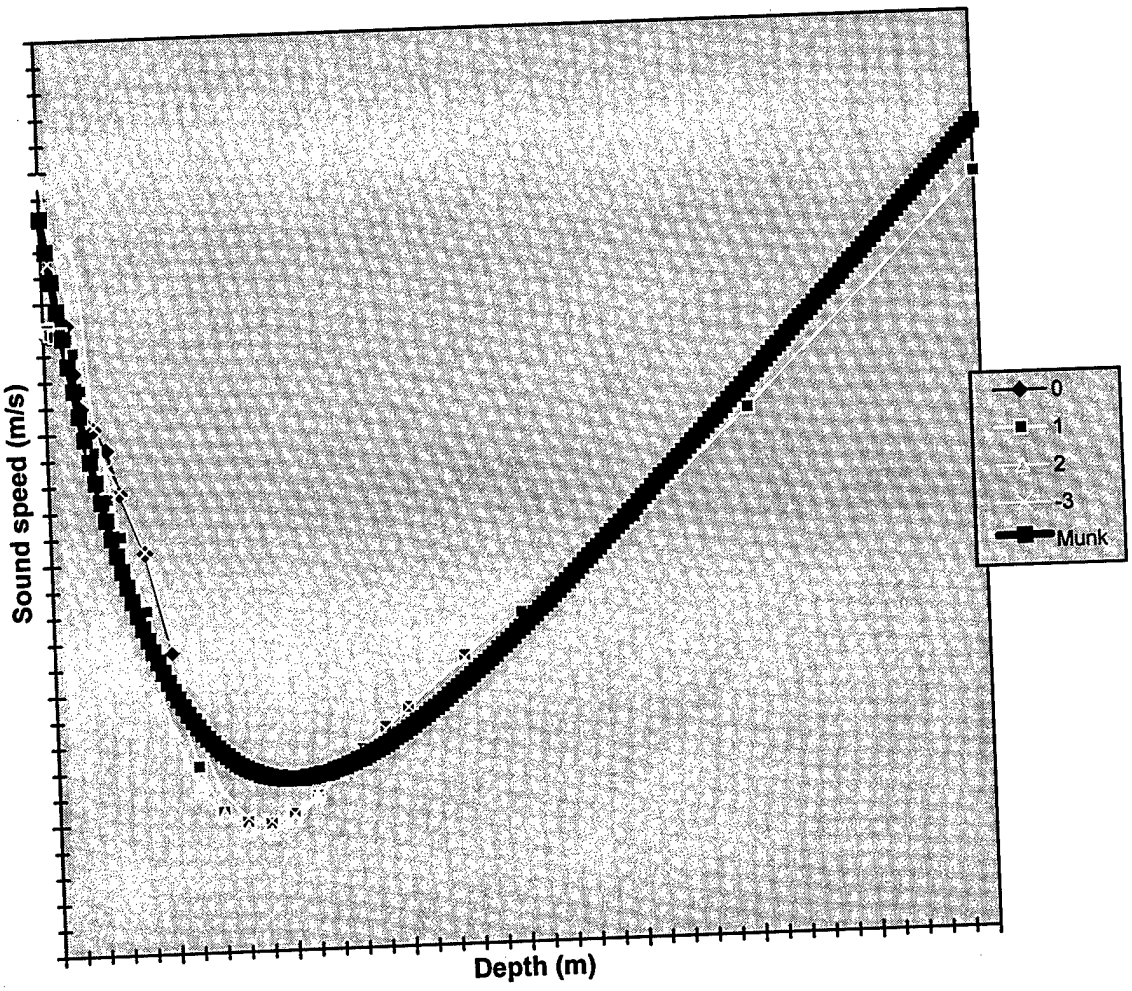

Latitude: 26S

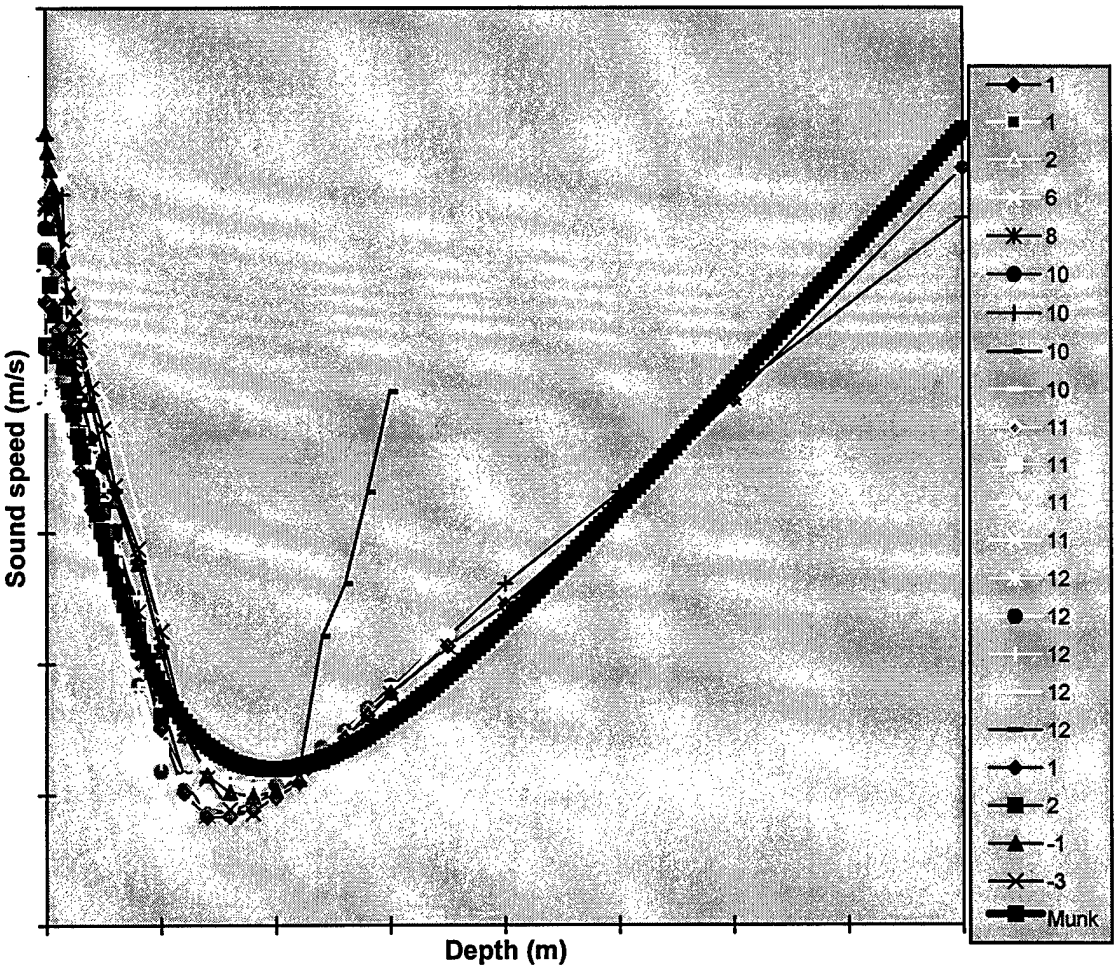

Latitude: 27S

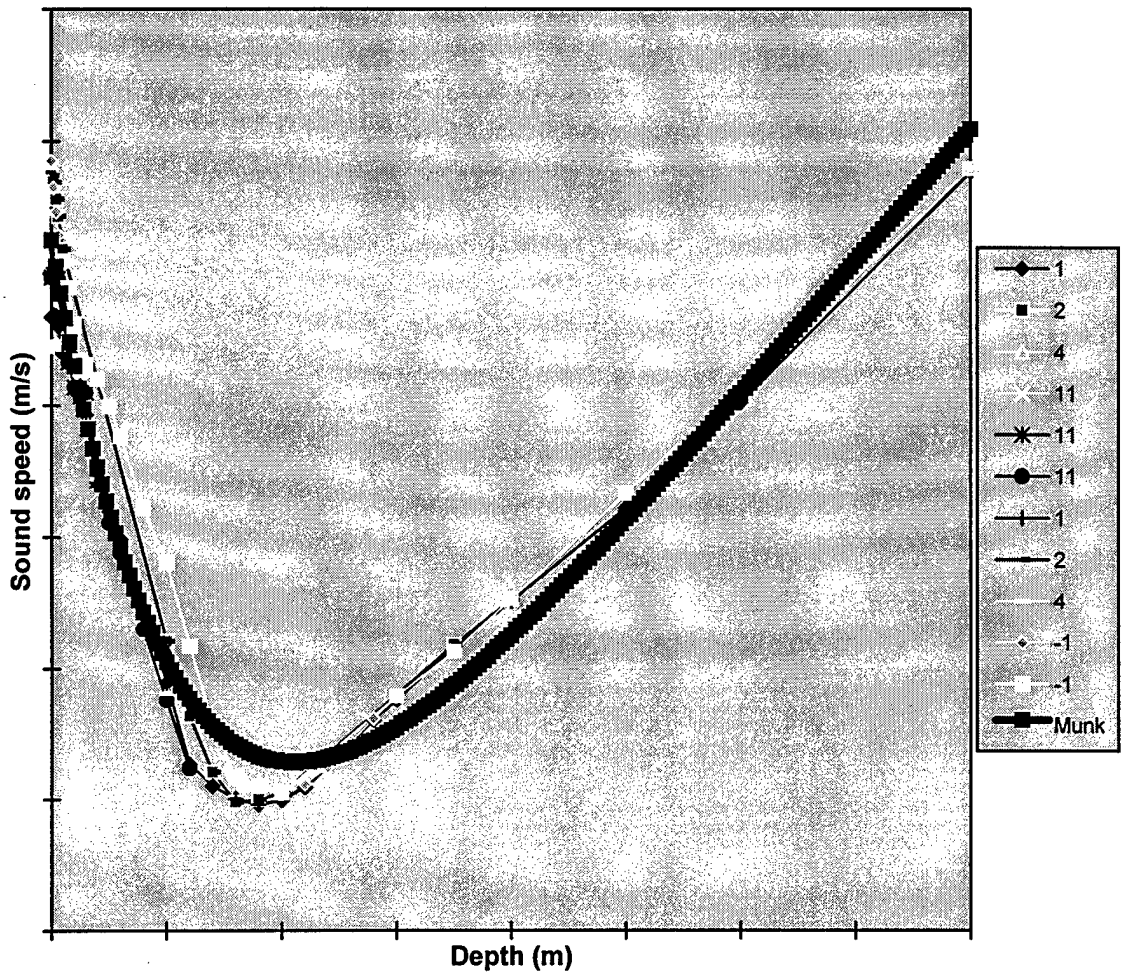

Latitude: 28S

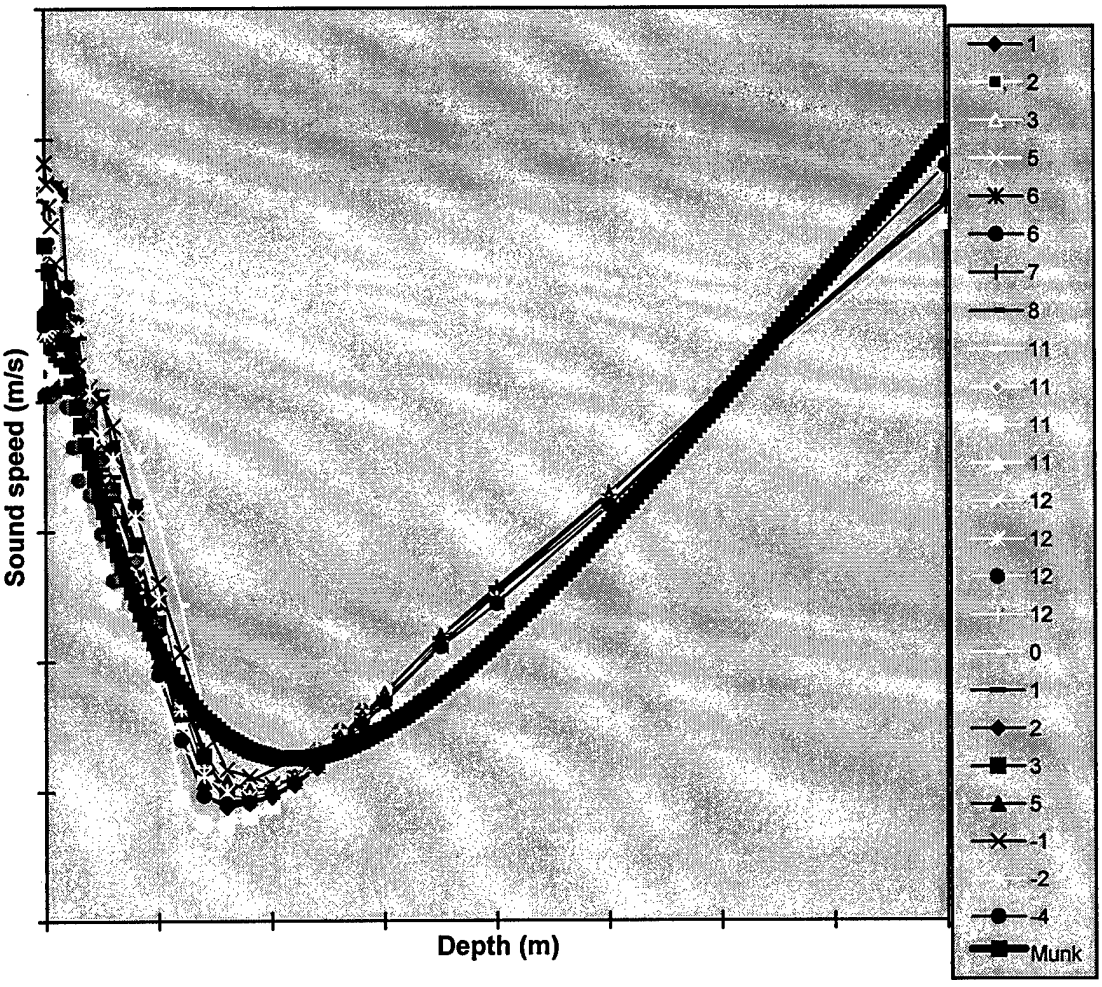

Latitude: 29S

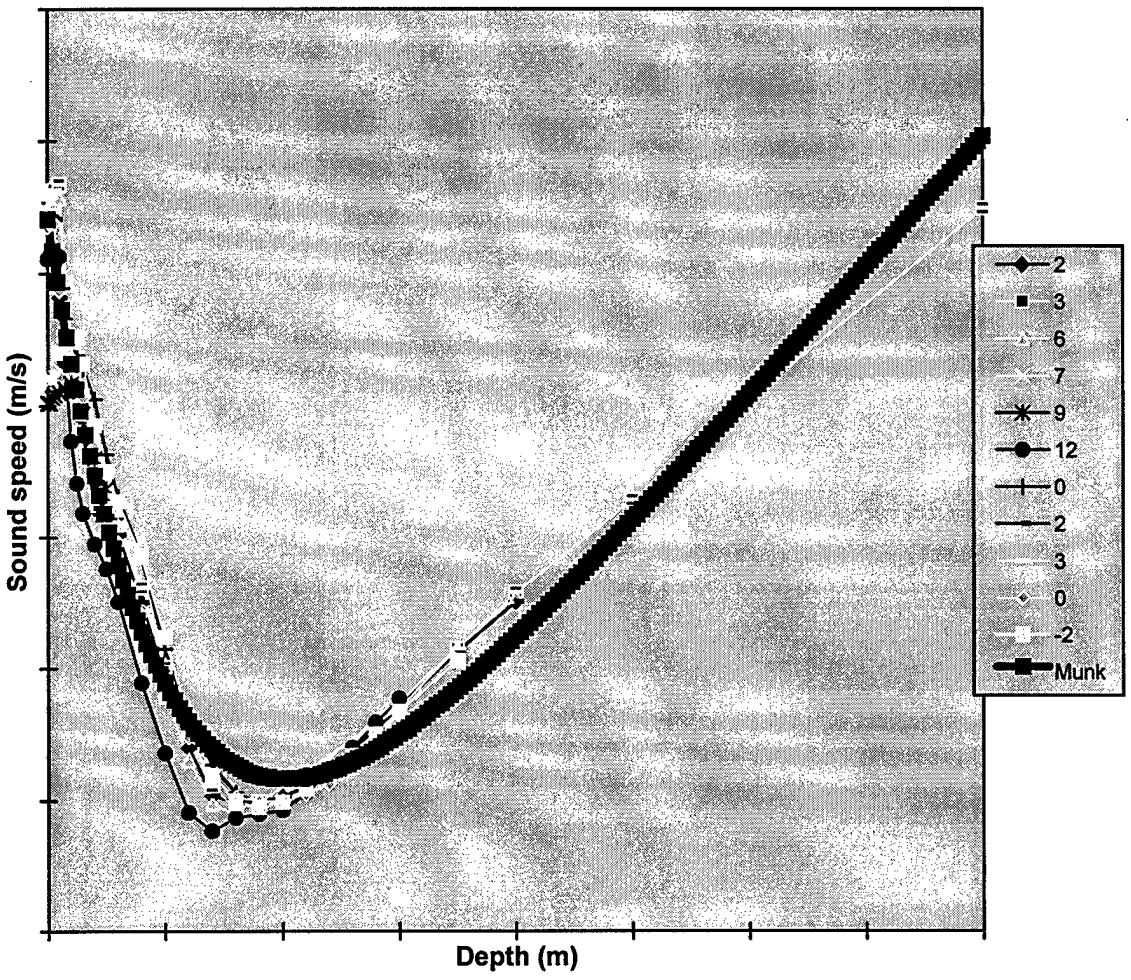

Latitude: 30S

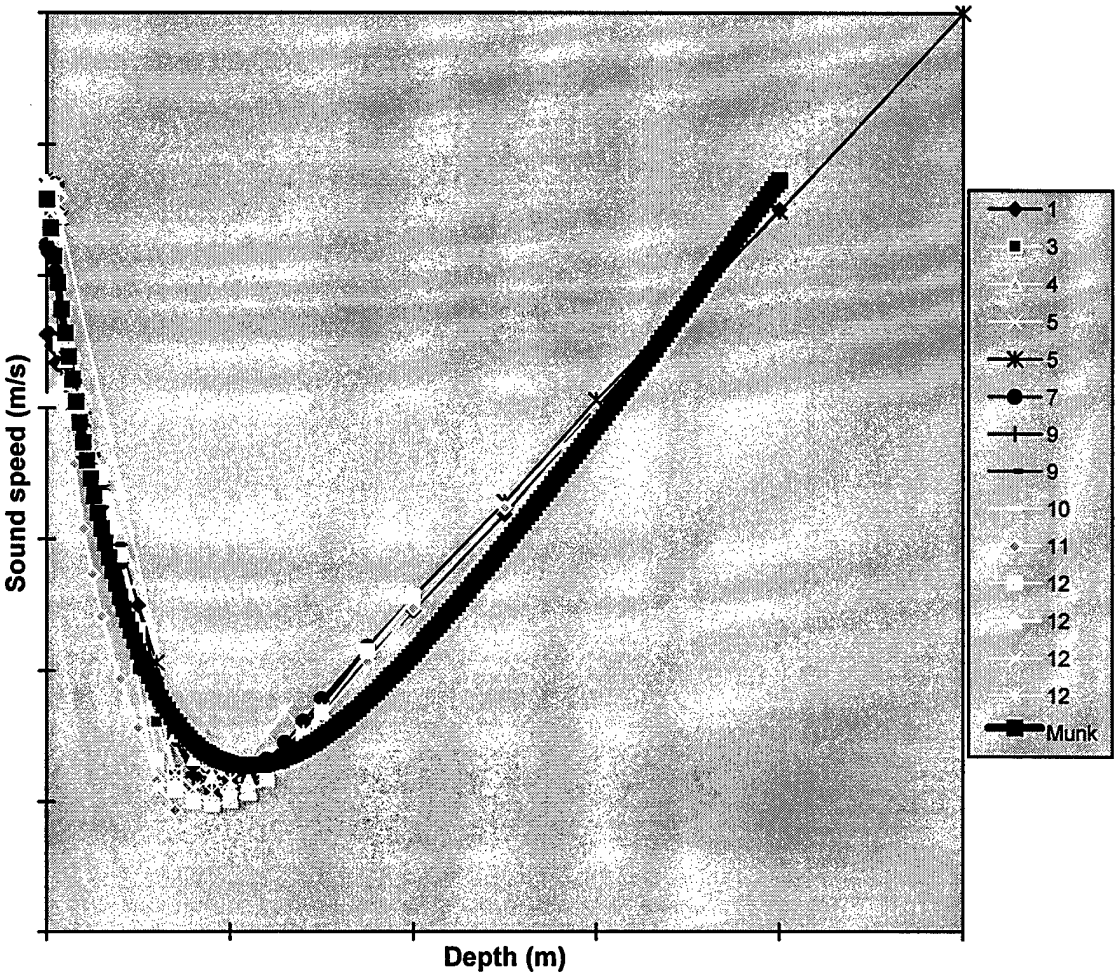

Latitude: 31 S

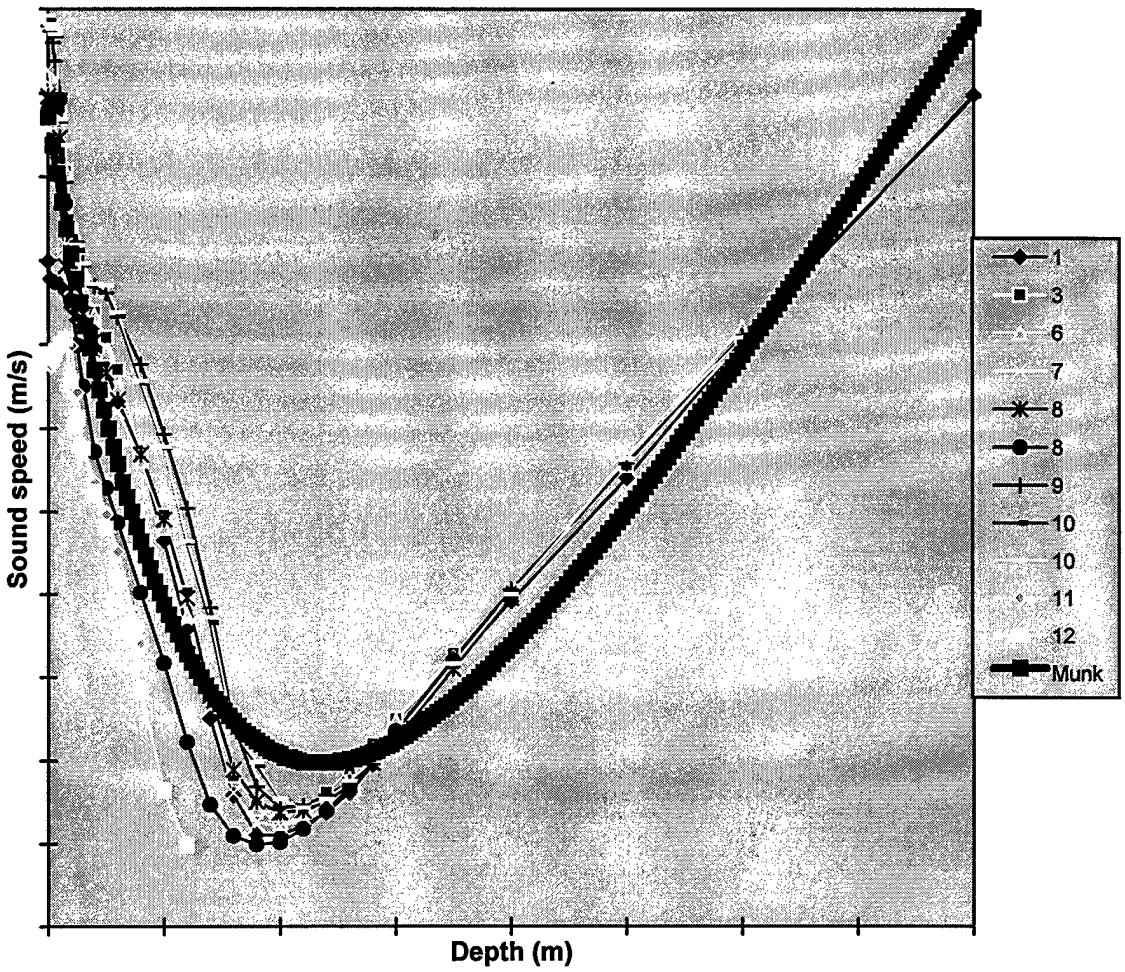

Latitude: 32S

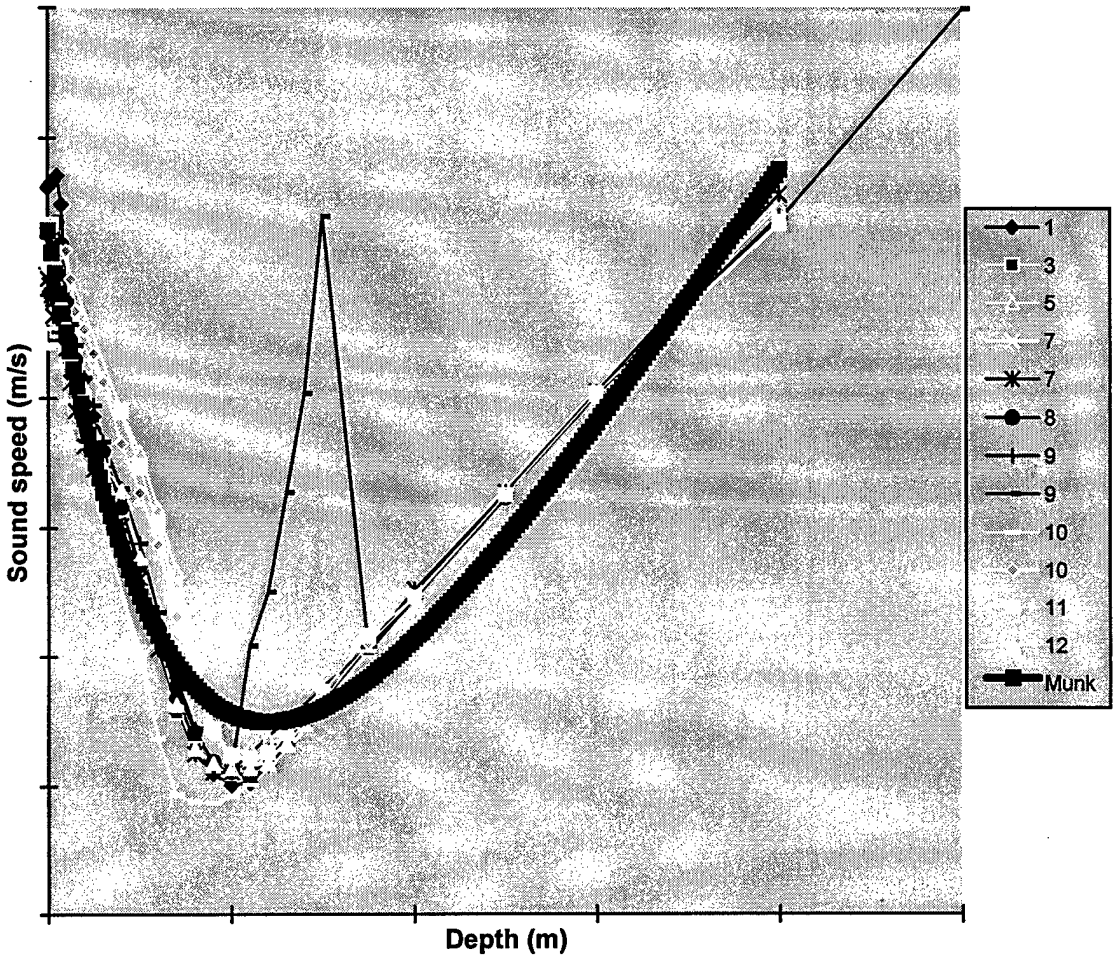

Latitude: 33S

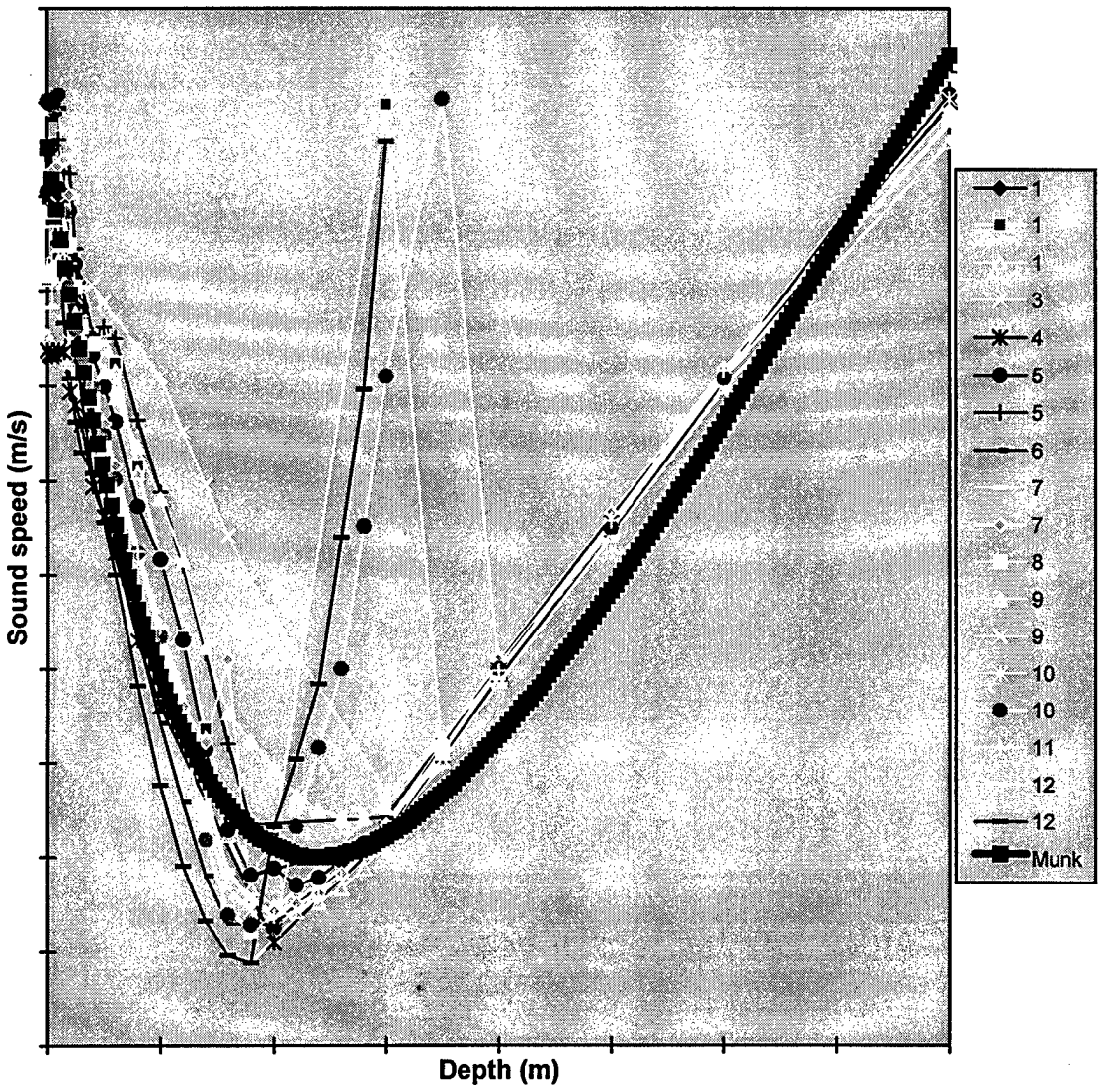

Latitude: 34S

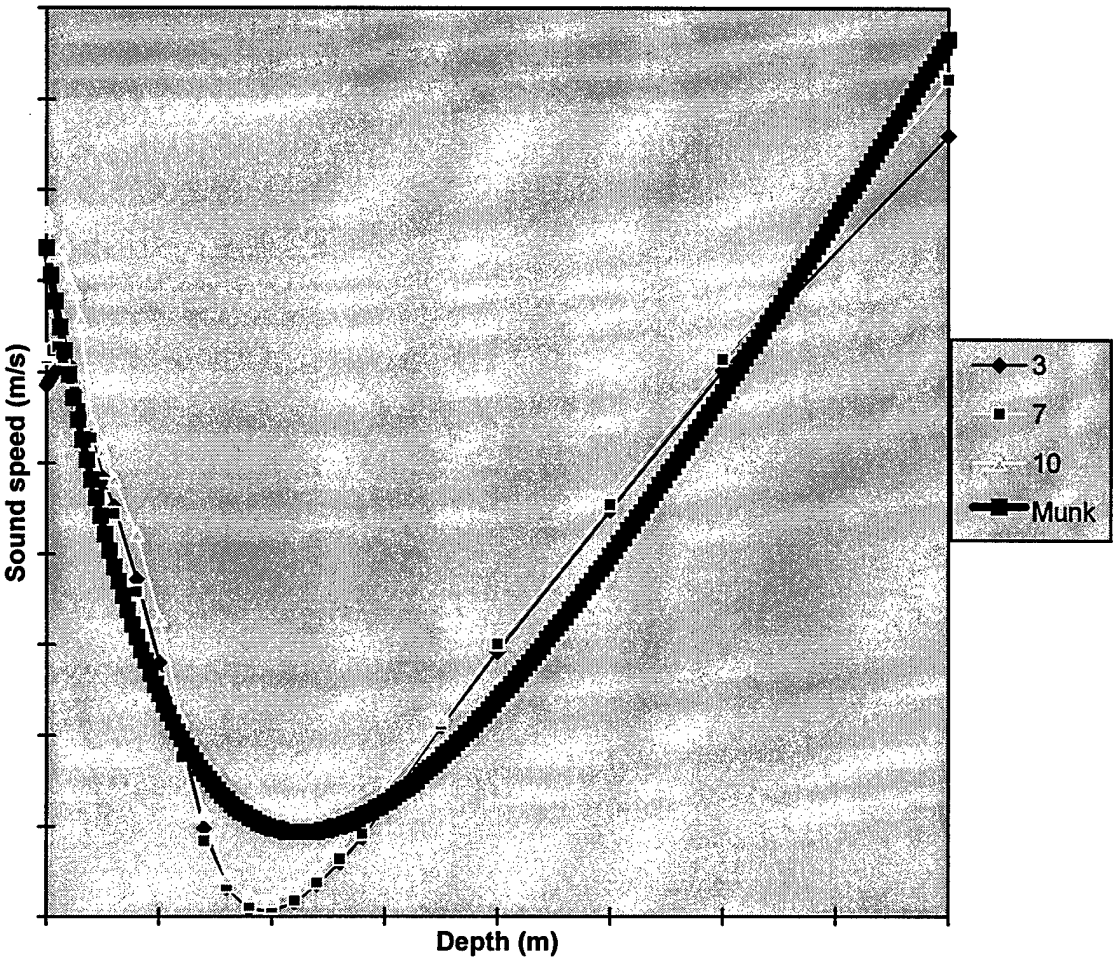

Latitude: 35S

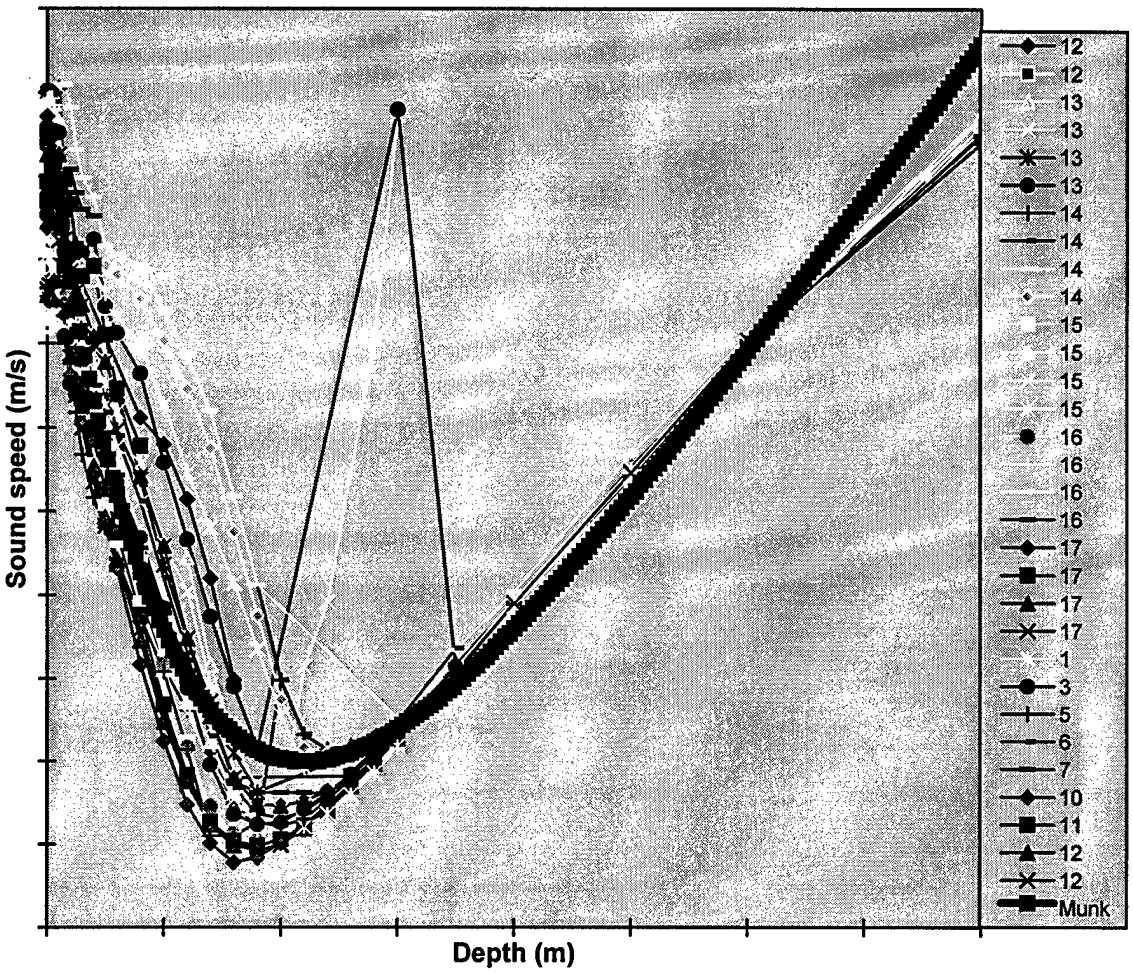

Latitude: 36S

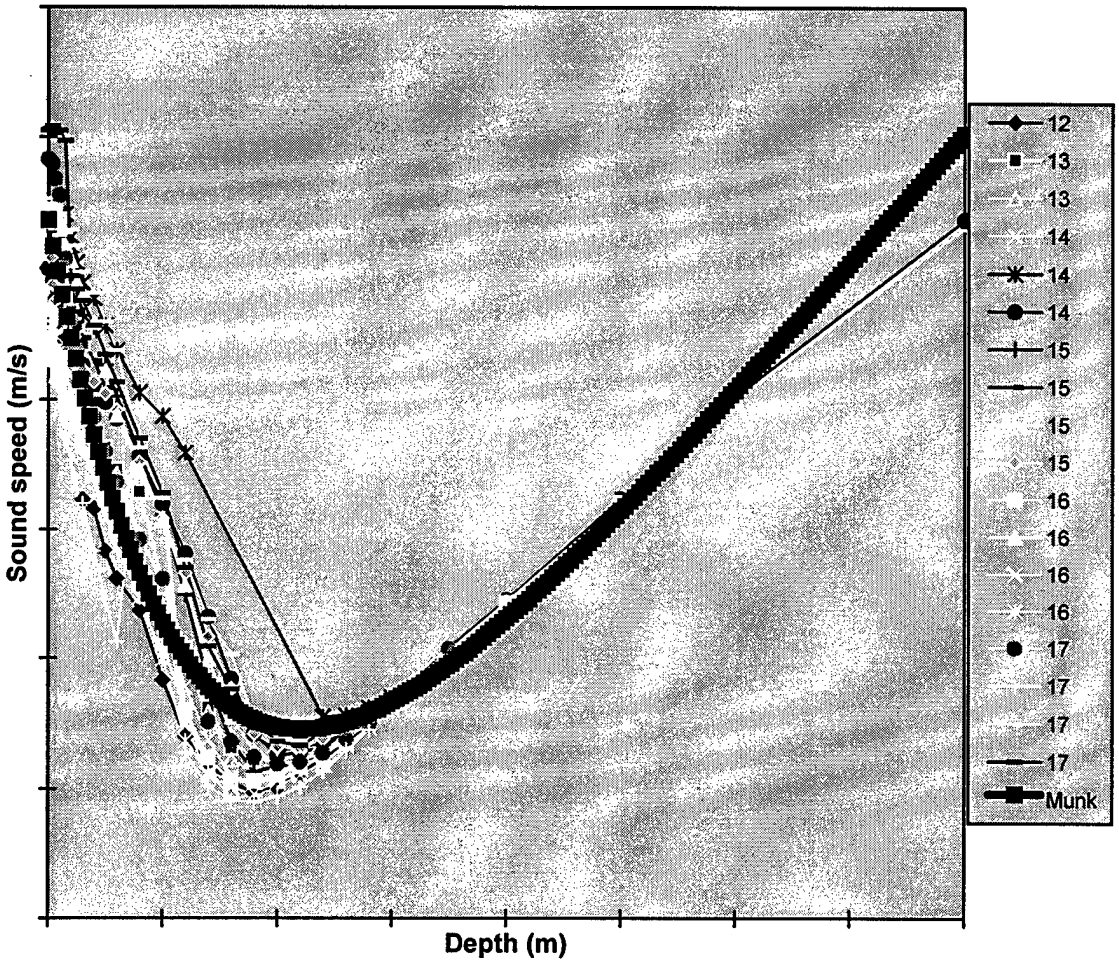

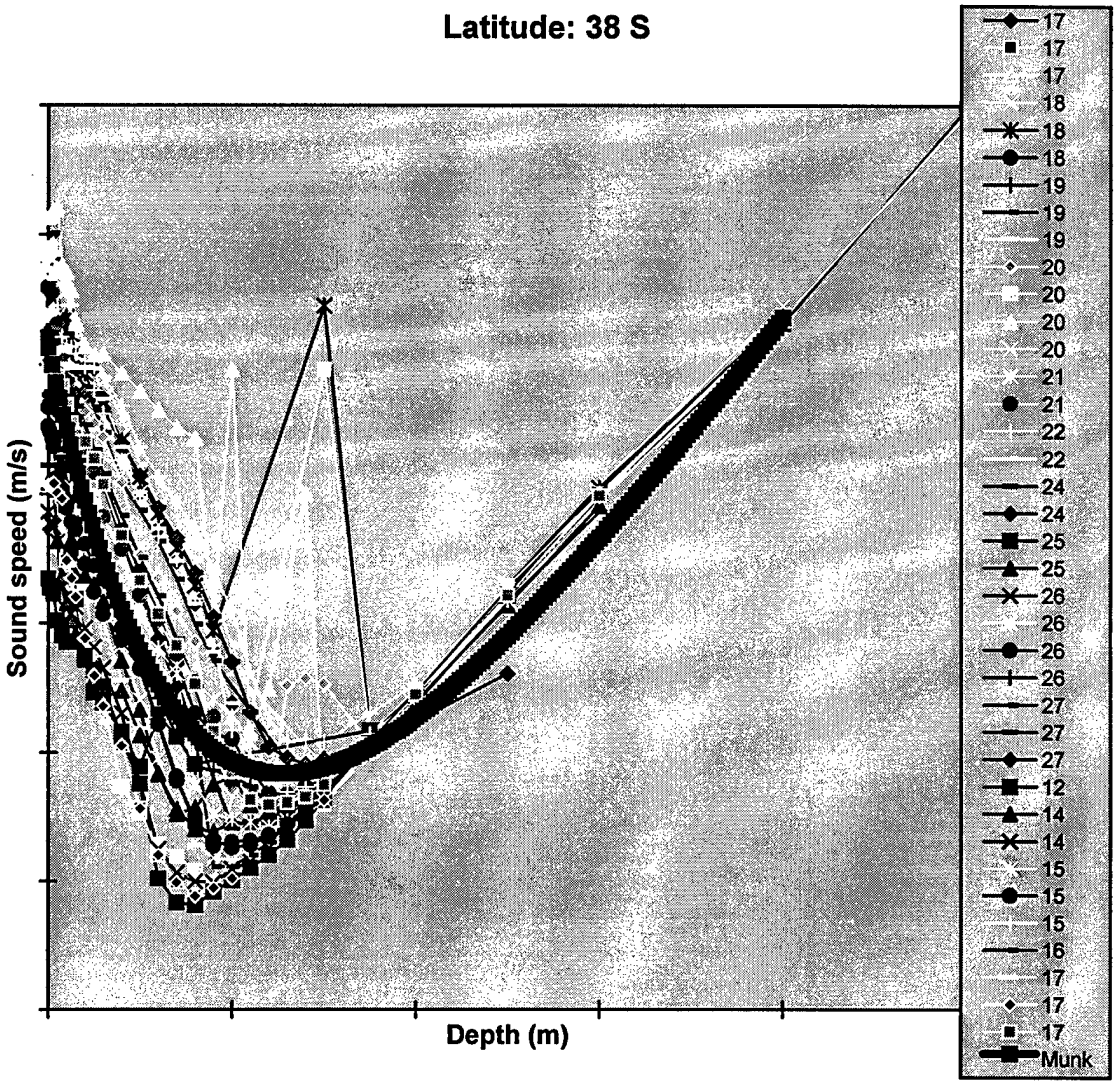
Latitude: 38 S
Sound speed (m/s)
Depth (m)
17
17
17
18
18
18
19
19
19
20
20
20
20
21
21
22
22
24
24
25
25
26
26
26
26
27
27
27
12
14
14
15
15
15
16
17
17
17
Munk

Latitude: 39S

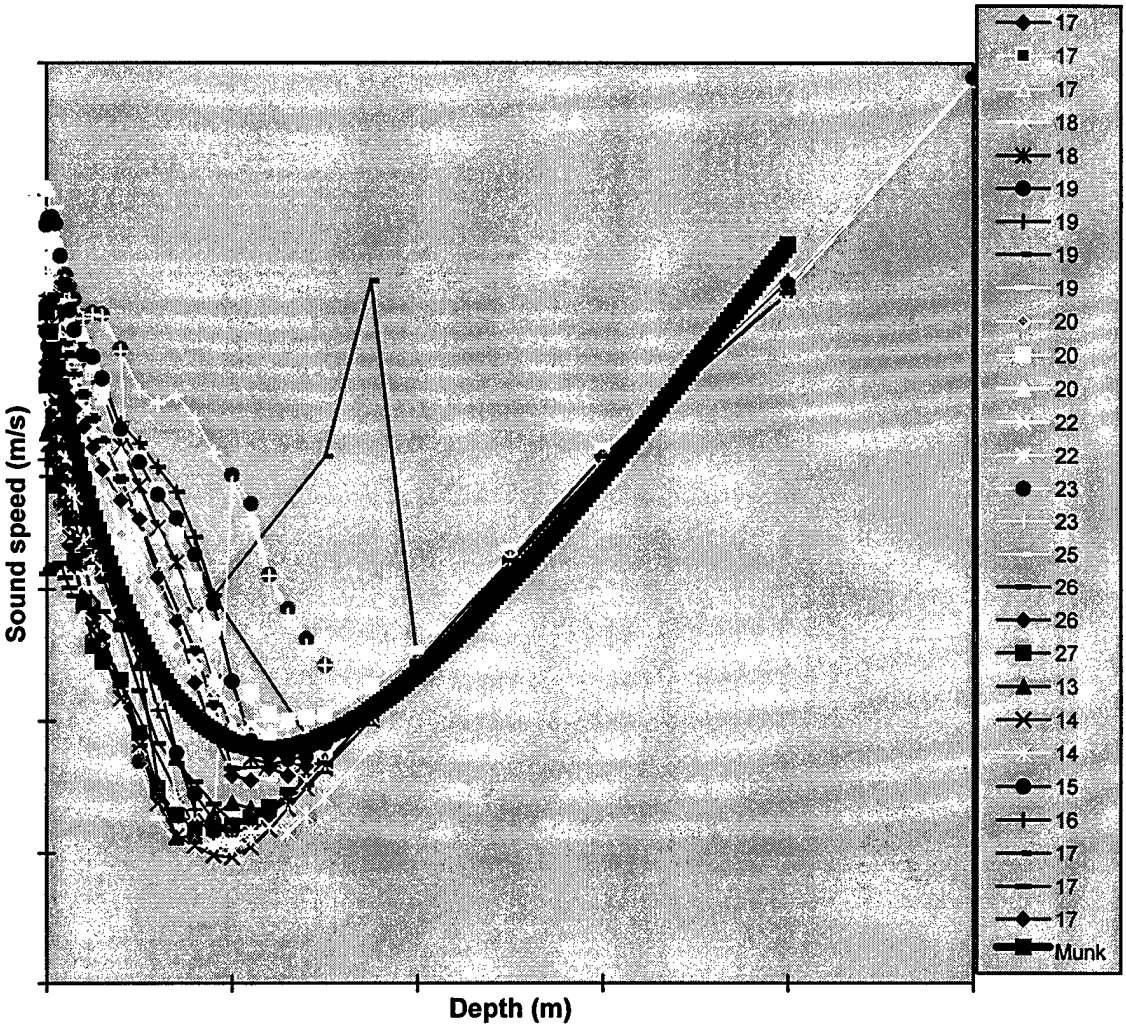

Latitude: 40S

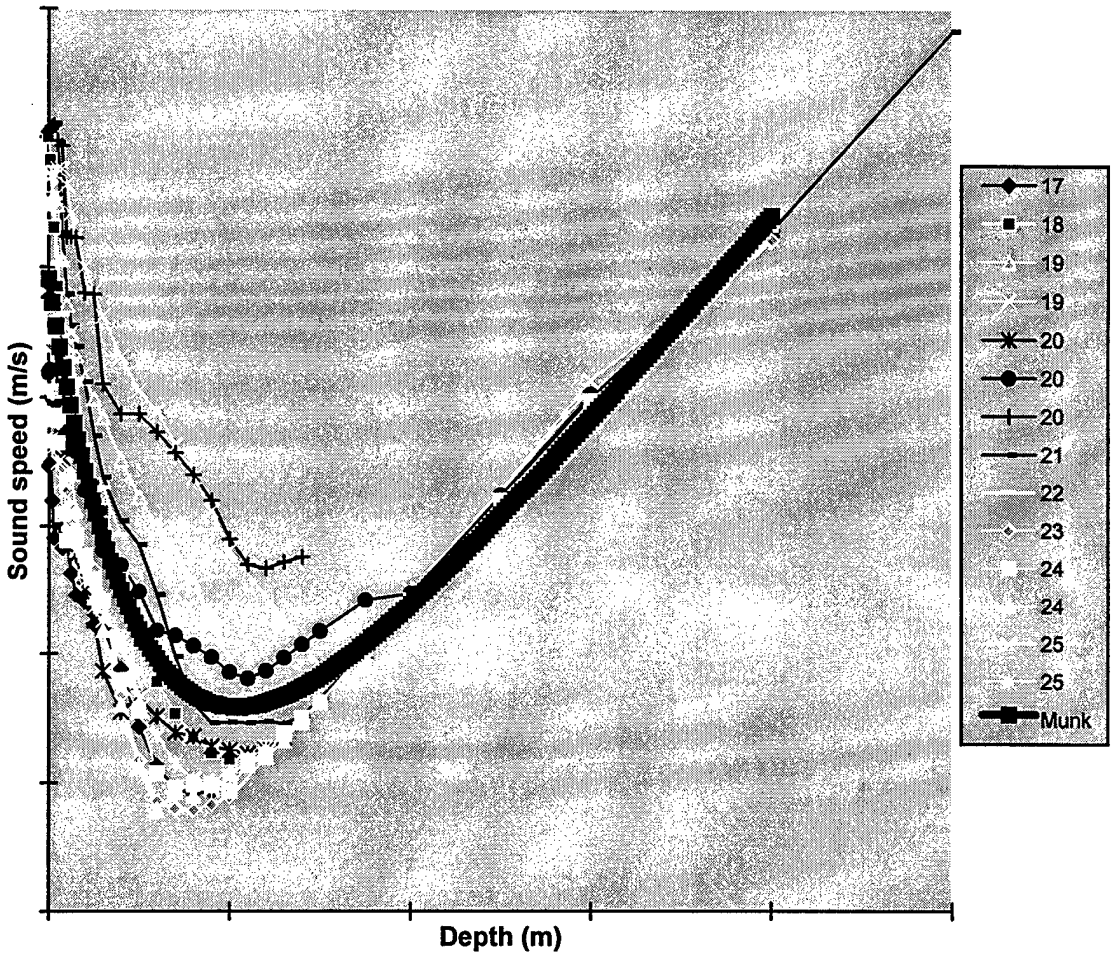

Latitude: 41S

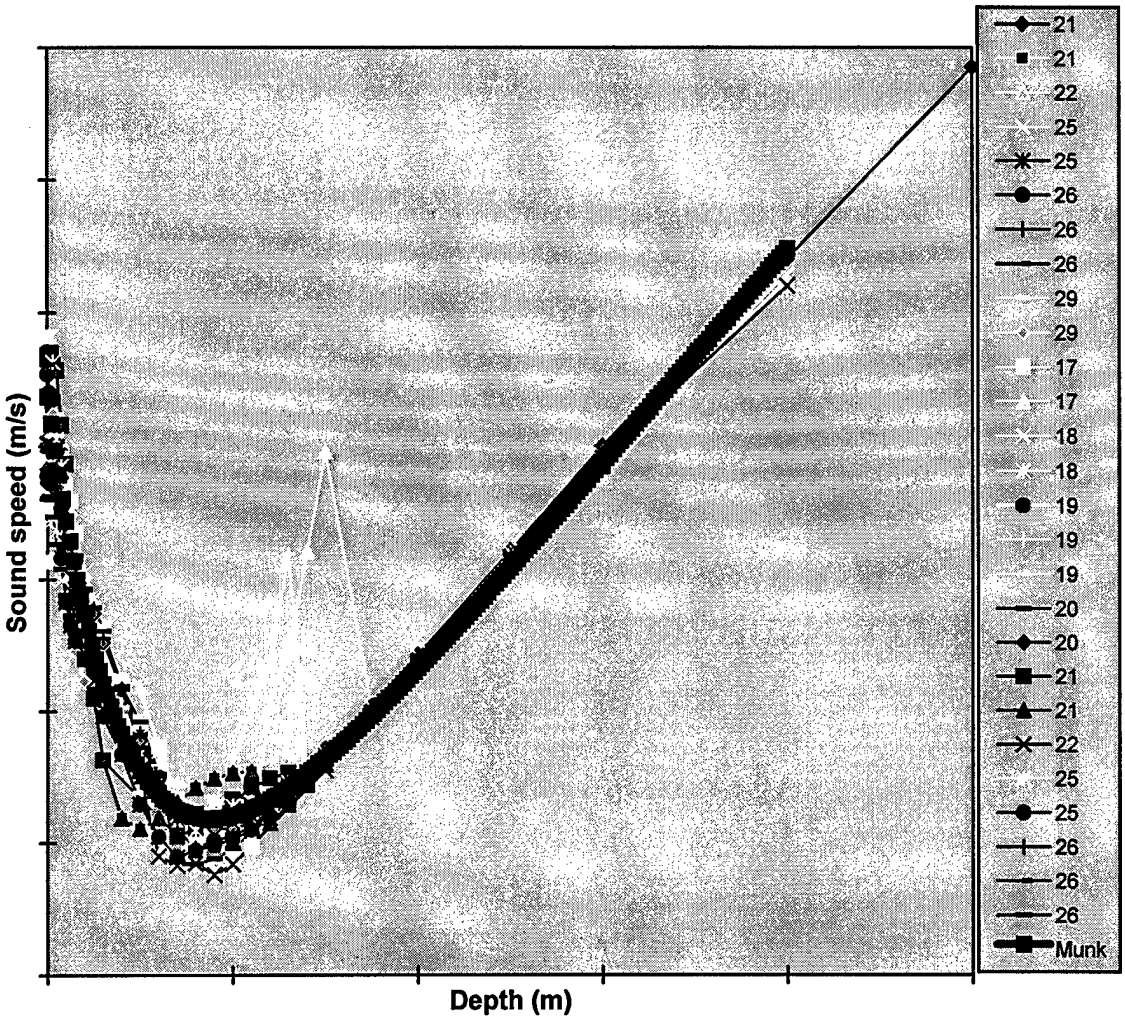

Latitude: 42S

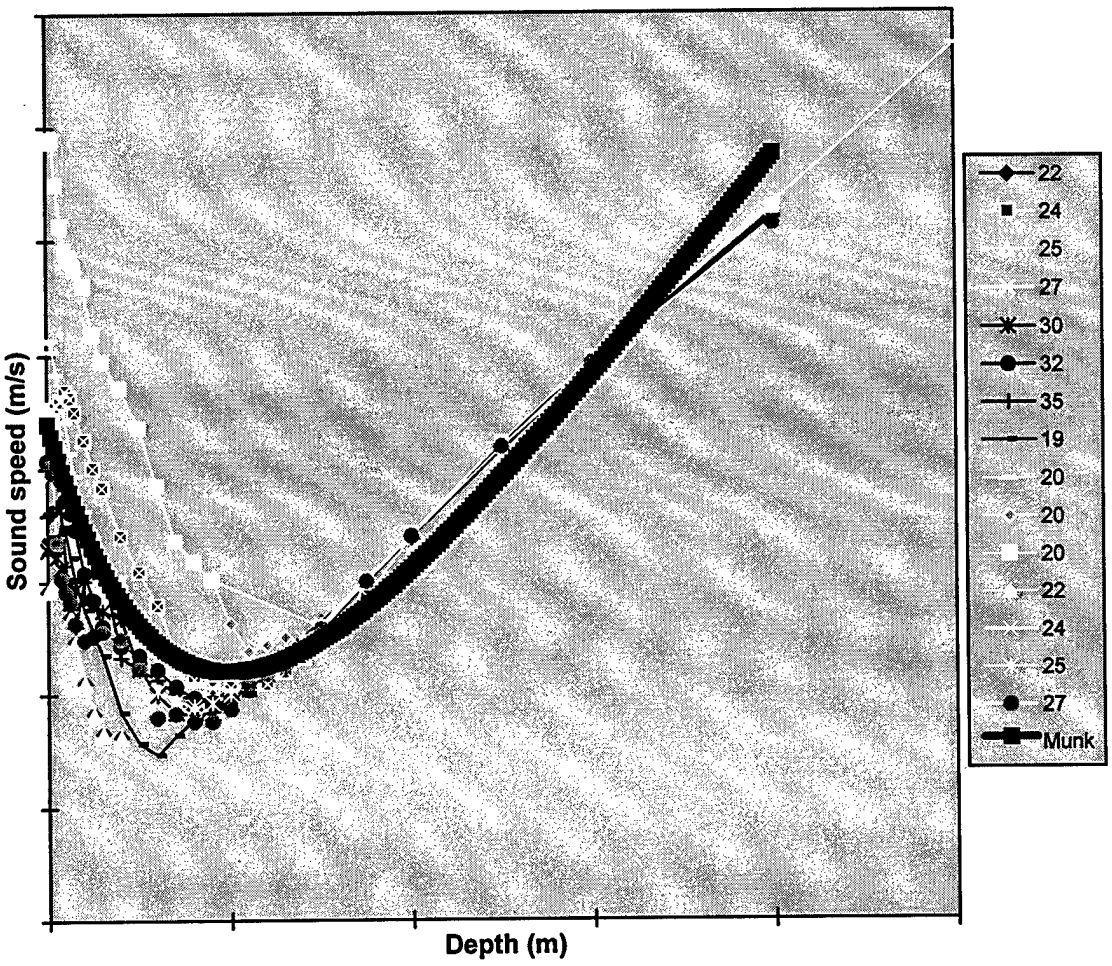

Latitude: 43S

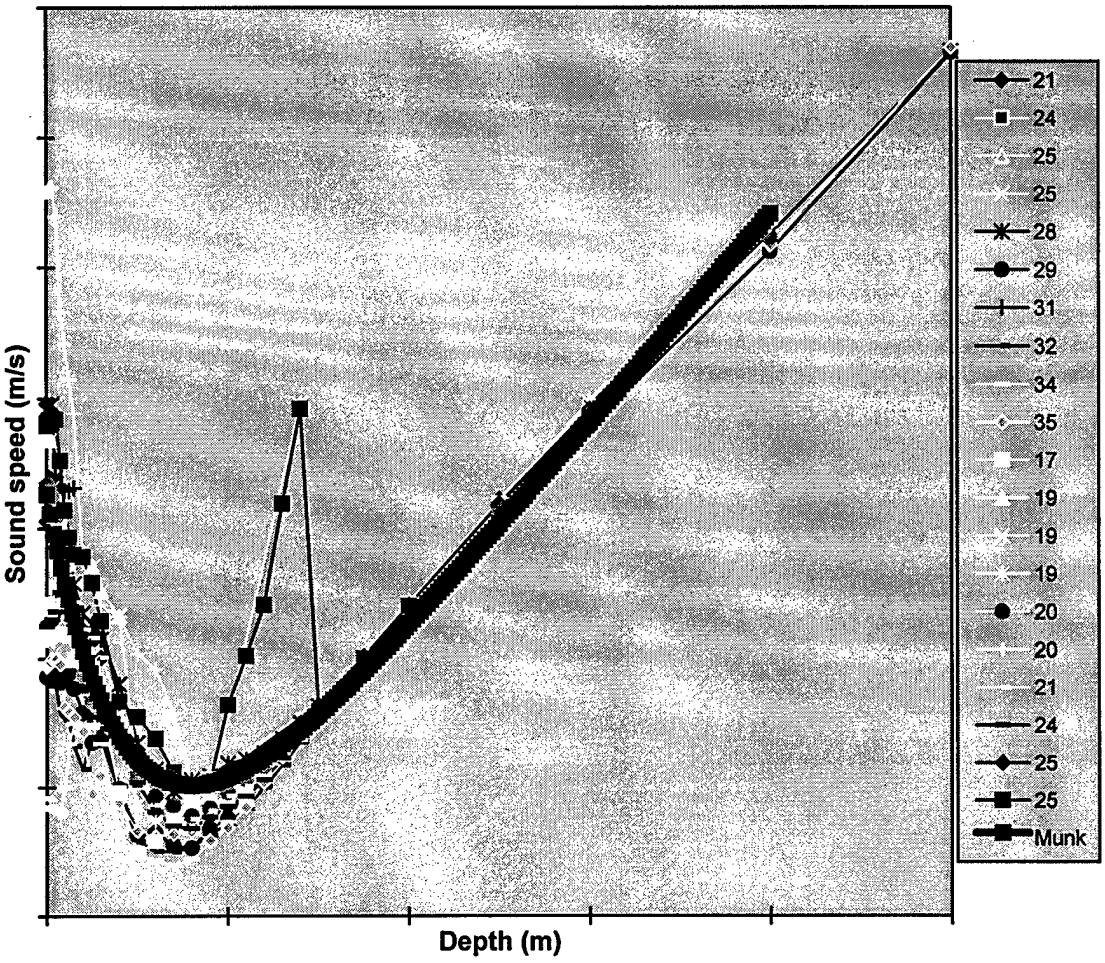

Latitude: 44S

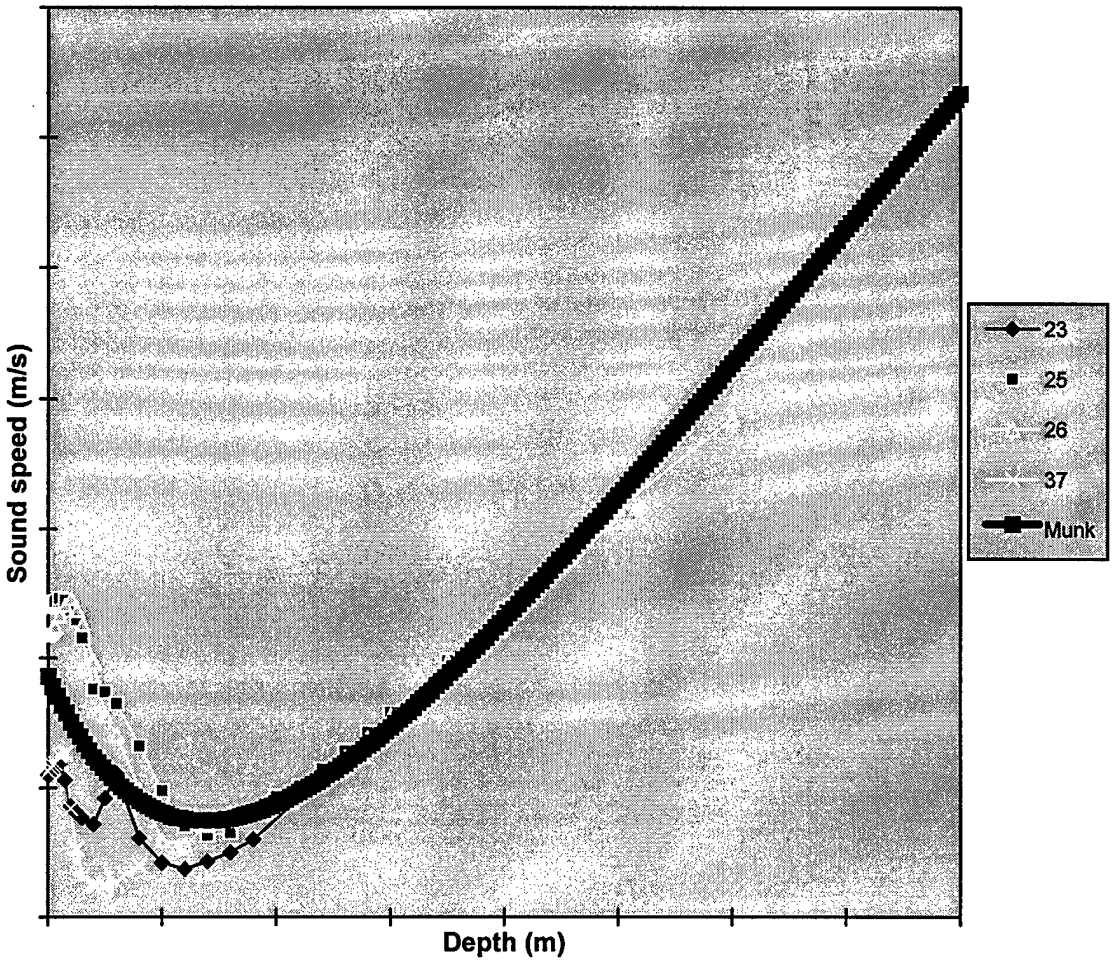

Latitude: 45S

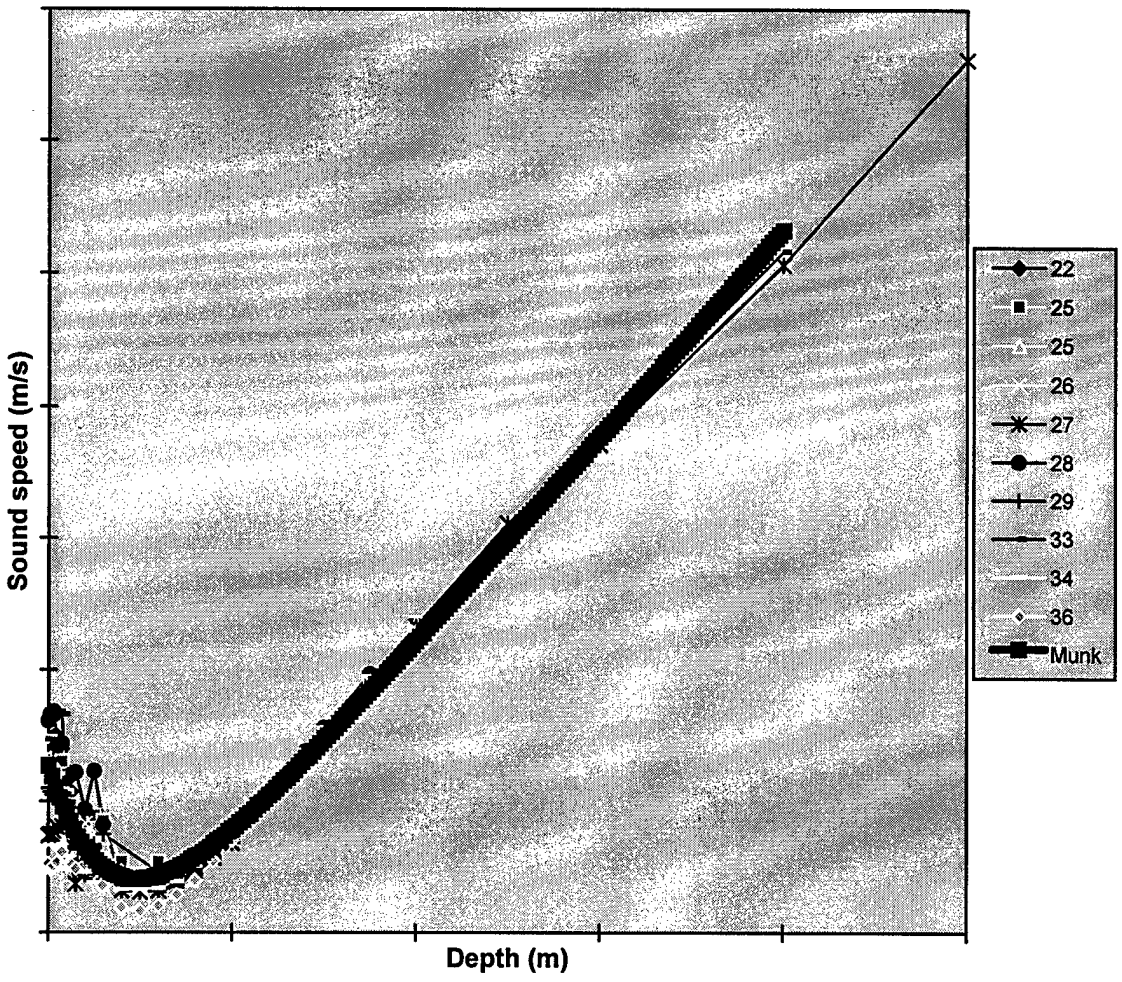

Latitude: 46S

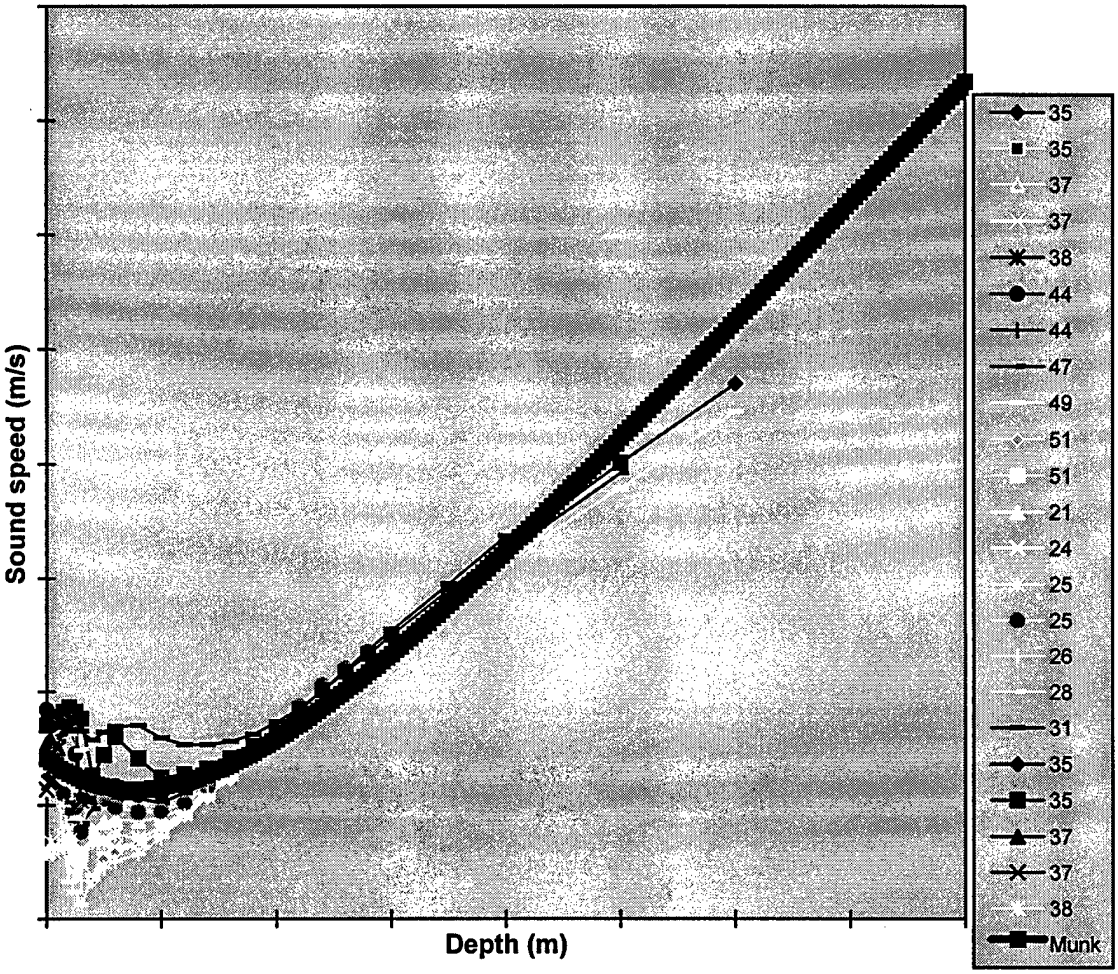

Latitude: 47S

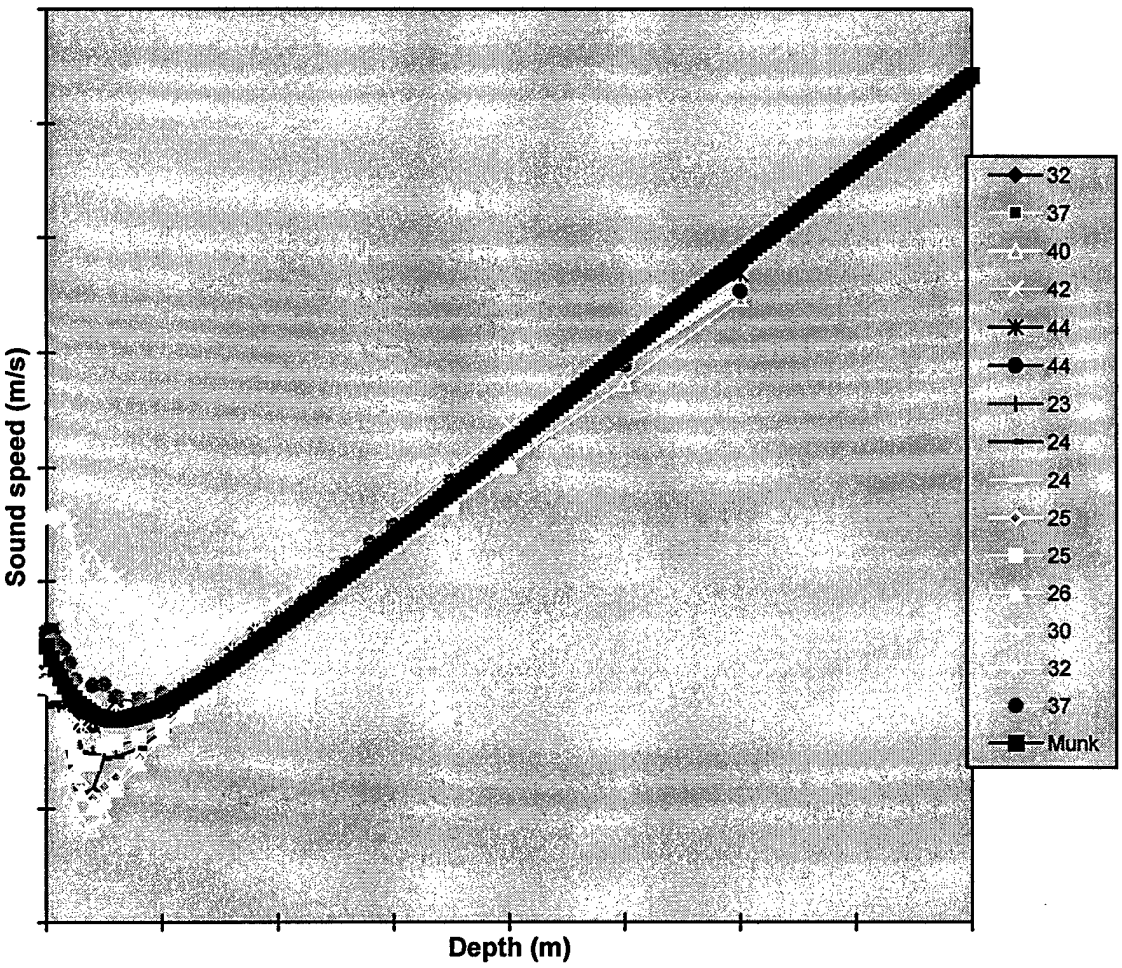

Latitude: 48S

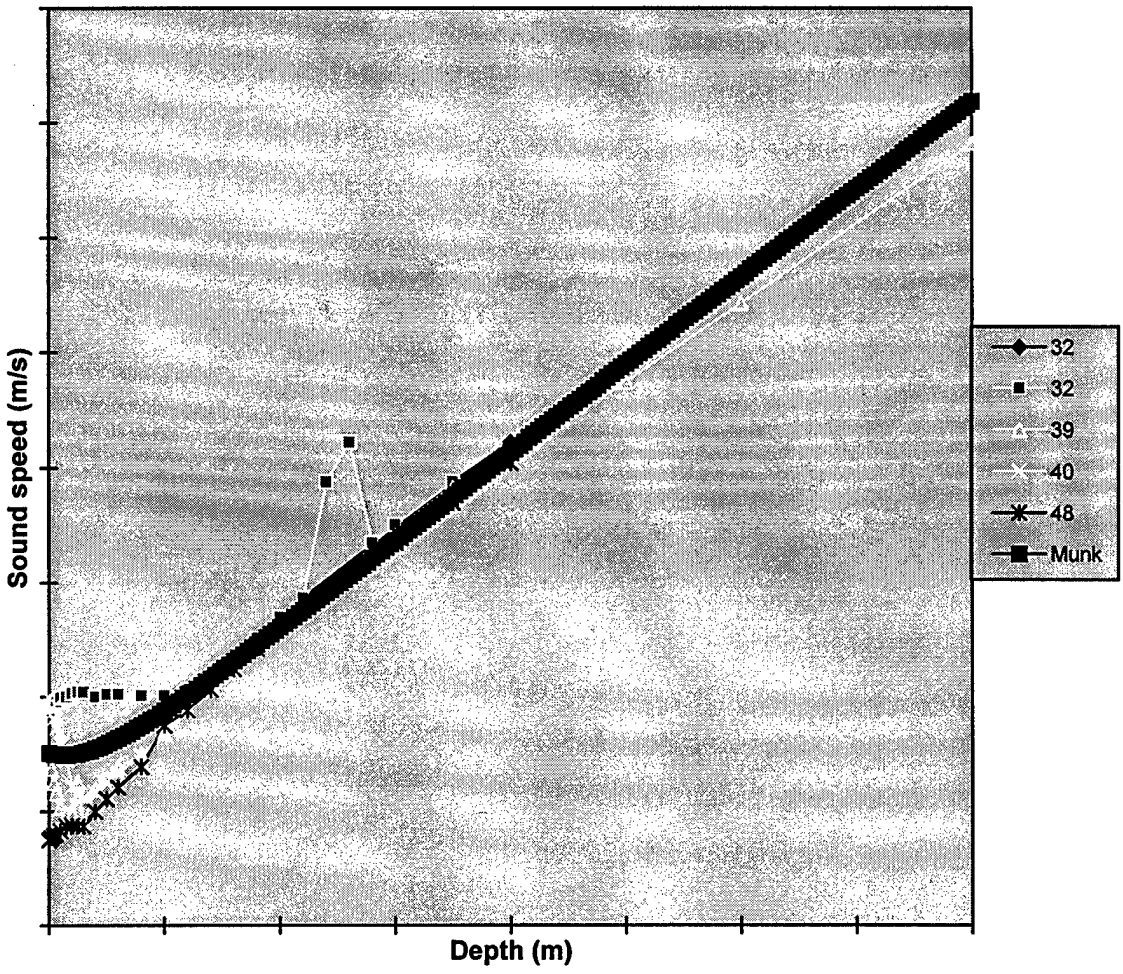

Latitude: 49S

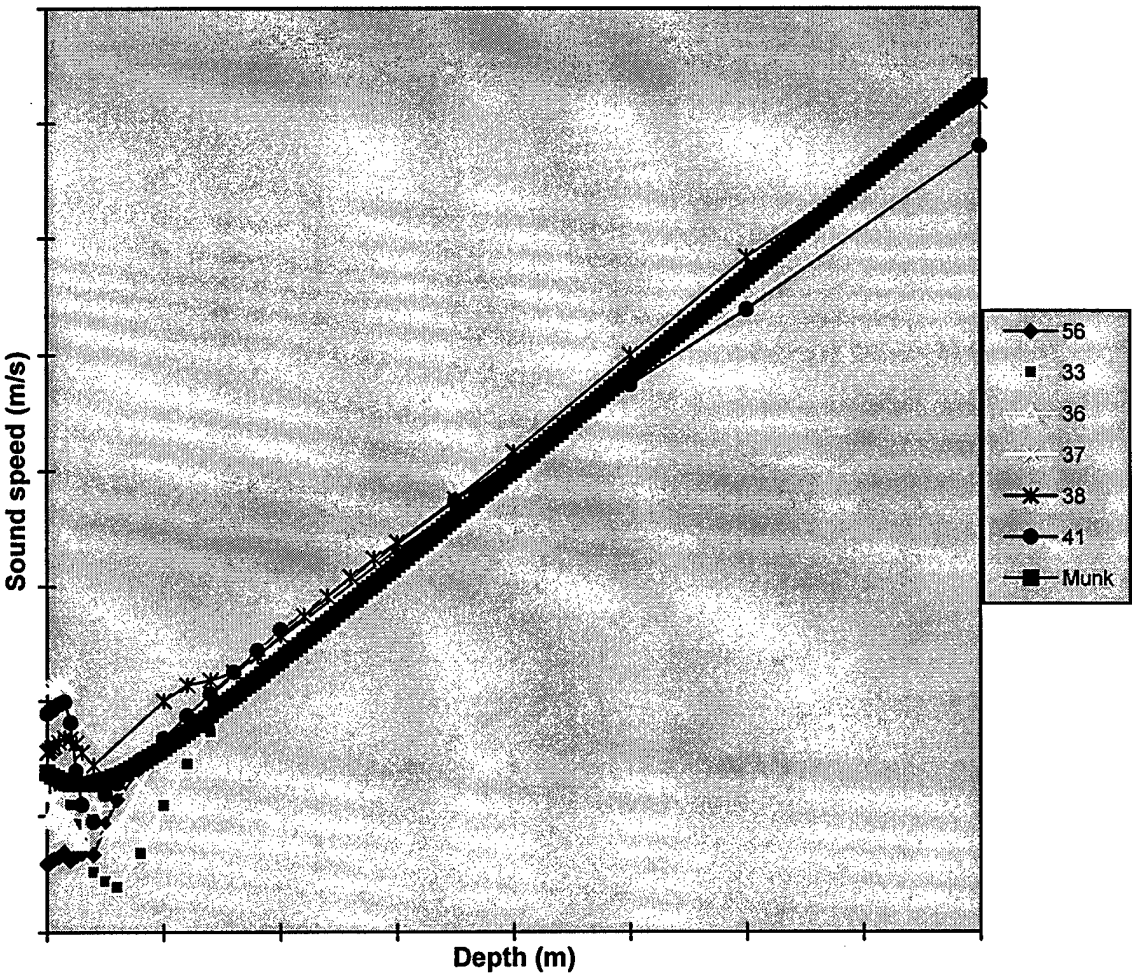

Latitude: 50S

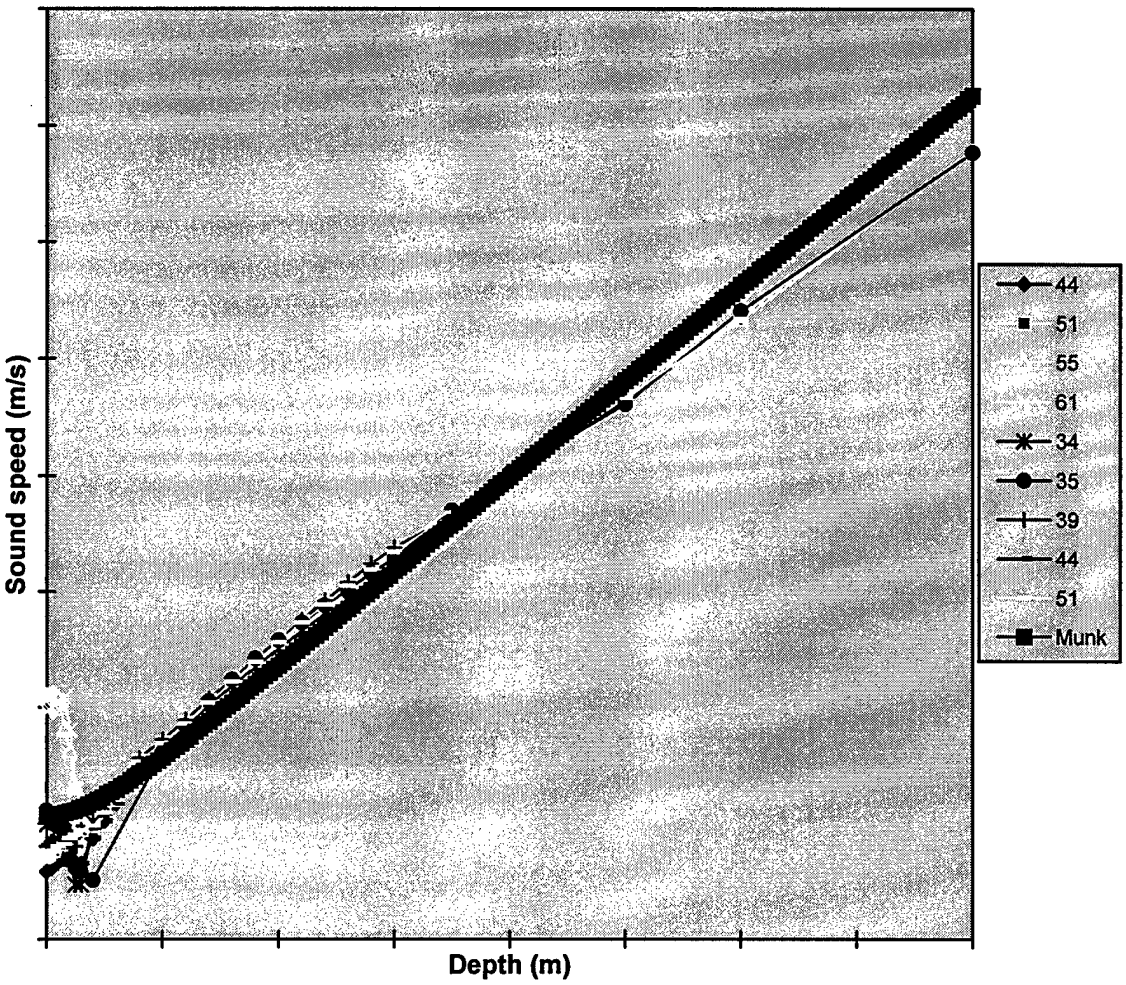

Latitude: 51S

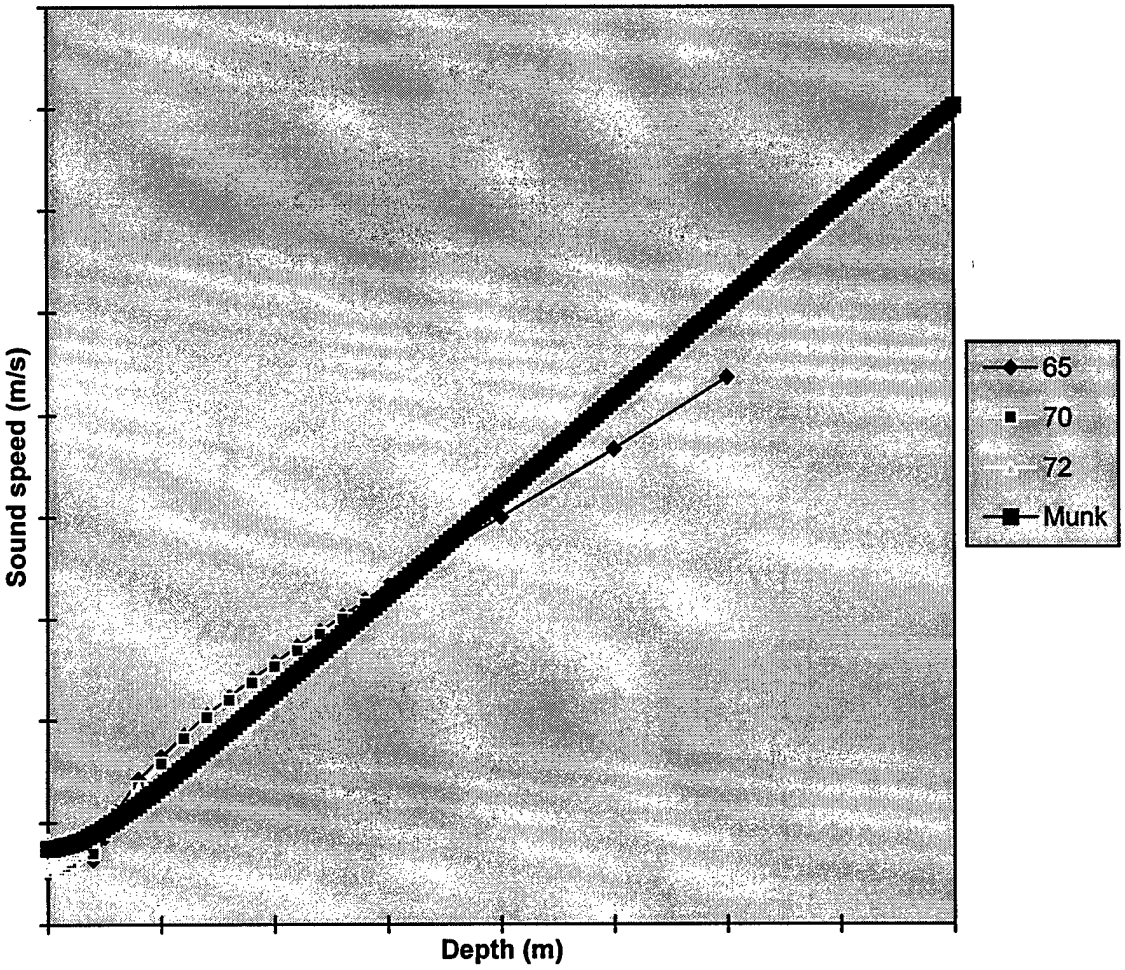

Latitude: 52 S